Journal of Volcanology and Geothermal Research 436 (2023) 107776

Contents lists available at ScienceDirect

Journal of Volcanology and Geothermal Research

journal homepage: www.journals.elsevier.com/journal-of-volcanology-and-geothermal-research

# Deep magma degassing and volatile fluxes through volcanic hydrothermal systems: Insights from the Askja and Kverkfjöll volcanoes, Iceland

Eemu Ranta [a,*], Sæmundur A. Halldórsson [a], Peter H. Barry [b], Shuhei Ono [c], Jóhann Gunnarsson Robin [a], Barbara I. Kleine [a,d], Andrea Ricci [e], Jens Fiebig [f], Árný E. Sveinbjörnsdóttir [a], Andri Stefánsson [a]

[a] Nordic Volcanological Center, Institute of Earth Sciences, University of Iceland, Sturlugata 7, 102, Reykjavik, Iceland
[b] Marine Chemistry and Geochemistry Department, Woods Hole Oceanographic Institution, 266 Woods Hole Road, Woods Hole, MA 02543, USA
[c] Department of Earth, Atmospheric and Planetary Sciences, Massachusetts Institute of Technology, 77 Massachusetts Avenue, Cambridge, MA 02139, USA
[d] GeoZentrum Nordbayern, Friedrich-Alexander-Universität Erlangen-Nuremberg, Schlossgarten 5, 91054 Erlangen, Germany
[e] Istituto Nazionale di Geofisica e Vulcanologia, Sezione di Palermo, Via Ugo La Malfa, 153, 90146 Palermo, Italy
[f] Institute of Geosciences, Goethe University, Altenhöferallee 1, 60438 Frankfurt/Main, Germany

ARTICLE INFO

*Keywords:*
Hydrothermal fluids
Stable isotopes
Magmatic volatiles
Magma degassing
Volatile fluxes
Iceland

ABSTRACT

Mantle volatiles are transported to Earth's crust and surface by basaltic volcanism. During subaerial eruptions, vast amounts of carbon, sulfur and halogens can be released to the atmosphere during a short time-interval, with impacts ranging in scale from the local environment to the global climate. By contrast, passive volatile release at the surface originating from magmatic intrusions is characterized by much lower flux, yet may outsize eruptive volatile quantities over long timescales. Volcanic hydrothermal systems (VHSs) act as conduits for such volatile release from degassing intrusions and can be used to gauge the contribution of intrusive magmatism to global volatile cycles. Here, we present new compositional and isotopic (δD and $\delta^{18}O$-$H_2O$, $^3He/^4He$, $\delta^{13}C$-$CO_2$, $\Delta^{33}S$-$\delta^{34}S$-$H_2S$ and $SO_4$) data for thermal waters and fumarole gases from the Askja and Kverkfjöll volcanoes in central Iceland. We use the data together with magma degassing modelling and mass balance calculations to constrain the sources of volatiles in VHSs and to assess the role of intrusive magmatism to the volcanic volatile emission budgets in Iceland.

The $CO_2/\Sigma S$ (10–30), $^3He/^4He$ (8.3–10.5 $R_A$; $^3He/^4He$ relative to air), $\delta^{13}C$-$CO_2$ (−4.1 to −0.2 ‰) and $\Delta^{33}S$-$\delta^{34}S$-$H_2S$ (−0.031 to 0.003 ‰ and −1.5 to +3.6‰) values in high-gas flux fumaroles ($CO_2$ > 10 mmol/mol) are consistent with an intrusive magmatic origin for $CO_2$ and S at Askja and Kverkfjöll. We demonstrate that deep (0.5–5 kbar, equivalent to ~2–18 km crustal depth) decompression degassing of basaltic intrusions in Iceland results in $CO_2$ and S fluxes of 330–5060 and 6–210 kt/yr, respectively, which is sufficient to account for the estimated $CO_2$ flux of Icelandic VHSs (3365–6730 kt/yr), but not the VHS S flux (220–440 kt/yr). Secondary, crystallization-driven degassing from maturing intrusions and leaching of crustal rocks are suggested as additional sources of S. Only a minor proportion of the mantle flux of Cl is channeled via VHSs whereas the $H_2O$ flux remains poorly constrained, because magmatic signals in Icelandic VHSs are masked by a dominant shallow groundwater component of meteoric water origin. These results suggest that the bulk of the mantle $CO_2$ and S flux to the atmosphere in Iceland is supplied by intrusive, not eruptive magmatism, and is largely vented via hydrothermal fields.

## 1. Introduction

Volatile fluxes from the mantle—a major reservoir of terrestrial volatiles (Bekaert et al., 2021)—to Earth's surface are mediated through the crust by volcanism. Long-term volcanic volatile fluxes are commonly extrapolated from direct measurements of volcanic gas plumes of erupting and persistently degassing volcanoes (e.g., Gerlach, 1991; Andres and Kasgnoc, 1998; Fischer, 2008; Aiuppa et al., 2019). However, intrusive basaltic magmatism delivers ~2–30 times more mantle-derived material to the crust than subaerial eruptions (White et al.,

* Corresponding author at: Department of Geoscience and Geography, University of Helsinki, Gustaf Hällströmin katu 2, 00560 Helsinki, Finland.
*E-mail address:* eemu.ranta@helsinki.fi (E. Ranta).

https://doi.org/10.1016/j.jvolgeores.2023.107776
Received 13 August 2022; Received in revised form 22 February 2023; Accepted 1 March 2023
Available online 6 March 2023

2006) and may supply an order of magnitude higher flux of key volatiles like $CO_2$ and S to the atmosphere (Gerlach, 1989). A major conduit of volatile transport between intrusions and the atmosphere are volcanic hydrothermal systems (VHSs), which may play a large, but relatively poorly constrained role in the global volatile cycles (e.g., Seward and Kerrick, 1996; McGee et al., 2001; Taran, 2009; Shinohara, 2013; Barry et al., 2014; Stefánsson et al., 2016b; Taran and Kalacheva, 2019; Fischer and Aiuppa, 2020). Such systems may further act as sinks of volatiles through mineralization reactions of, for example, sulfides and carbonates, or, conversely, facilitate leaching of volatiles from the shallow country rocks.

Volcanic hydrothermal systems are powered by magmatic intrusions that heat the surrounding groundwater that percolates through porous or fractured rocks to the surface, giving rise to thermal surface manifestations such as hot springs, fumaroles, acid lakes and steaming grounds. Considerable efforts through the last century have been made to constrain the sources of the main volatile species present in such hydrothermal fluids ($H_2$, $H_2O$, B, $CO_2$, $CH_4$, $N_2$, Cl, $H_2S$, $SO_2$, noble gases) (Craig, 1963; Sakai and Matsubaya, 1977; Marty and Giggenbach, 1990; Giggenbach, 1992; Sano and Marty, 1995; Stefánsson et al., 2017; Gunnarsson-Robin et al., 2017; Fiebig et al., 2019; Labidi et al., 2020; Ricci et al., 2022). Some of the least melt-soluble volatiles, such as $CO_2$ and He, are likely to be mainly sourced from magmas, whereas others, like the heavy noble gases (Ne-Ar-Kr-Xe; Füri et al., 2010; Byrne et al., 2021) and N (Labidi et al., 2020) are mainly of atmospheric origin. More melt-soluble elements like B and Cl are thought to be derived in large part from the host rocks through fluid-rock reactions ('leaching'), whereas volatiles with intermediate solubility, like S may be sourced from both leaching and magmatic degassing (e.g., Stefánsson et al., 2015; Gunnarsson-Robin et al., 2017). VHSs in Iceland—a subaerial portion of the mid-Atlantic ridge—are typically associated with active central volcanoes and caldera structures, where shallow (~2–6 km) magmatic intrusions provide the heat sources that drive hydrothermal circulation along faults and through porous, volcanic bed rock. These shallow intrusions likely represent the top of a multi-tier 'ladder' of intrusions that extends through the crust to the mantle (Maclennan, 2019; White et al., 2019), potentially providing a deep supply of magmatic gases to the overlying VHSs. Thus, Icelandic VHSs provide an opportunity to study the mantle-to-atmosphere transport of volatiles at a divergent plate boundary.

Here, we present major and trace element, stable isotope (δD, $\delta^{18}O$, $\delta^{13}C$, $\Delta^{33}S$, $\delta^{34}S$) and helium isotope ($^3He/^4He$) data for thermal and non-thermal waters and fumarole gases from the active Askja and Kverkfjöll volcanic systems, located in the Northern Rift Zone (NRZ) of Iceland (Figs. 1 and 2). These locations are advantageous for studying magmatic volatile input into VHSs, as the pre-eruptive volatile elemental and isotopic characteristics of basalts from the area are well constrained by data from glassy silicate melt inclusions and subglacially erupted pillow glasses (Barry et al., 2014; Hartley et al., 2021; Matthews et al., 2021; Marshall et al., 2022; Ranta et al., 2022; Ranta, 2022), and because the local crust—a major source of volatiles in many hydrothermal areas worldwide—is dominantly basaltic and volatile-poor. Further, the aquifers at Askja and Kverkfjöll are devoid of seawater, which is a major source of $H_2O$, B, Cl and S, and thus complicates the detection of magmatic signals in coastal and submarine VHSs (Stefánsson et al., 2017). We use our geochemical dataset, along with estimated magmatic gas compositions for three main purposes: (1) to evaluate which geochemical signals in surface thermal fluids are derived from magmatic gases emanating from crustal intrusions, (2) to determine the relative contributions of magmatic, crustal and meteoric sources of volatiles to VHSs and (3) to constrain the shallow and deep fluxes of mantle-derived volatiles to the atmosphere channeled via VHSs in Iceland.

## 2. Geological setting

The Northern Rift Zone (NRZ) of Iceland (Fig. 1a) is a subaerial portion of the divergent plate boundary that separates the Eurasian and North American tectonic plates. The Askja and Kverkfjöll volcanoes are located in the southern part of the NRZ in the Central Highlands, both hosting relatively unexplored high-temperature hydrothermal areas (Ármannsson, 2016).

Kverkfjöll is a mature volcanic system at the SE end of the NRZ. It comprises a central stratovolcano, partly covered by the Vatnajökull ice cap, and a connecting fissure swarm (Fig. 2b). Kverkfjöll is considered to be an active volcano with dozens of basaltic eruptions during the Holocene, although no historical (<1100 yr) eruptions are known (Óladóttir et al., 2011). A vigorous hydrothermal system at Kverkfjöll is manifested on the surface at several locations around the 3 × 8 km large and 100 m deep, ice-filled NE caldera (Figs. 1d, 2). A large vapor-dominated hydrothermal area is centered along a fault on the NW caldera rim at 1550–1700 m elevation. This area is divided into the three separate areas Efri and Neðri Hveradalur, and Hveratagl, that together host dozens of individual fumaroles, boiling pots, mud pools and several ice caves, as well as two ice-dammed hydrothermal lakes Galtarlón and Gengissig (Thórarinsson, 1953; Ólafsson et al., 2000; Oddsson, 2016) (Figs. 1d, 2).

Hydrothermal explosions have occurred at Gengissig and its vicinity in 1959, 1968 and 2013 (Montanaro et al., 2016). Two thermal rivers, Volga and Hveragil, flow down the southern and eastern caldera rims, respectively. Their flow rates are approximately 100–200 L/s for Volga (prior to spring snow melting) and 200–250 L/s for Hveragil (Oddsson, 2016), with temperatures of up to ~26 °C and ~62 °C, respectively (Ólafsson et al., 2000, this study). Hveragil is characterized by up to 0.5 m thick, layered carbonate travertine deposits along its banks (Fig. 2a). Minor hydrothermal activity has been occasionally observed as hot vapor or heated grounds on the high slopes of the steep NE cliffs of the caldera and close to the highest top Jörfi (1933 m.a.s.l.) (Thórarinsson, 1953; Ólafsson et al., 2000). However, no anomalous temperatures were detected with an infrared camera by Oddsson (2016), who considered geothermal activity in the NE caldera to be subordinate compared to the other hydrothermal manifestations. Oddsson (2016) concluded that the total hydrothermal heat output of Kverkfjöll amounts to 265 ± 72 MW spread over a hydrothermal area of 2–2.5 $km^2$.

Askja is a bimodal and productive volcanic system comprising a fissure swarm and a central volcano. The last eruption of Askja, in 1961, was a relatively small basaltic fissure eruption on the eastern caldera rim that formed the Vikrahraun lava field (Thórarinsson and Sigvaldason, 1962). The latest-formed of its four nested calderas formed following a rhyolitic VEI 5 eruption in 1875 (Hartley and Thordarson, 2012) and is occupied by the 10.7 $km^2$ large and up to 217 m deep Lake Öskjuvatn (~1052 m.a.s.l). The main hydrothermal activity at Askja is at present found in three areas around Lake Öskjuvatn: Víti and Bátshraun in the NE, at Suðurbotnar to the SE and at Mývetningahraun and below Þorvaldstindur in the SW (Fig. 3c; Jónasson and Einarsson, 2009). The Suðurbotnar hydrothermal area was partly covered by a large landslide in July 2014 (Gylfadóttir et al., 2017). The hydrothermal activity extends to the Öskjuvatn lake, at least to a depth of 80 m (Ólafsson, 1980), but its full extent and distribution on the lake floor are not well known. A hydrothermal explosion crater Víti, formed in connection to the 1875 eruption (Sparks et al., 1981), today hosts an acid thermal lake and several moderately active fumaroles. Both the 1875 and 1961 eruptions were preceded by increased fumarolic activity (Thórarinsson and Sigvaldason, 1962).

## 3. Methods

### 3.1. Sampling and major element analysis

A total of 16 fumarole discharge samples, 13 thermal waters and 8

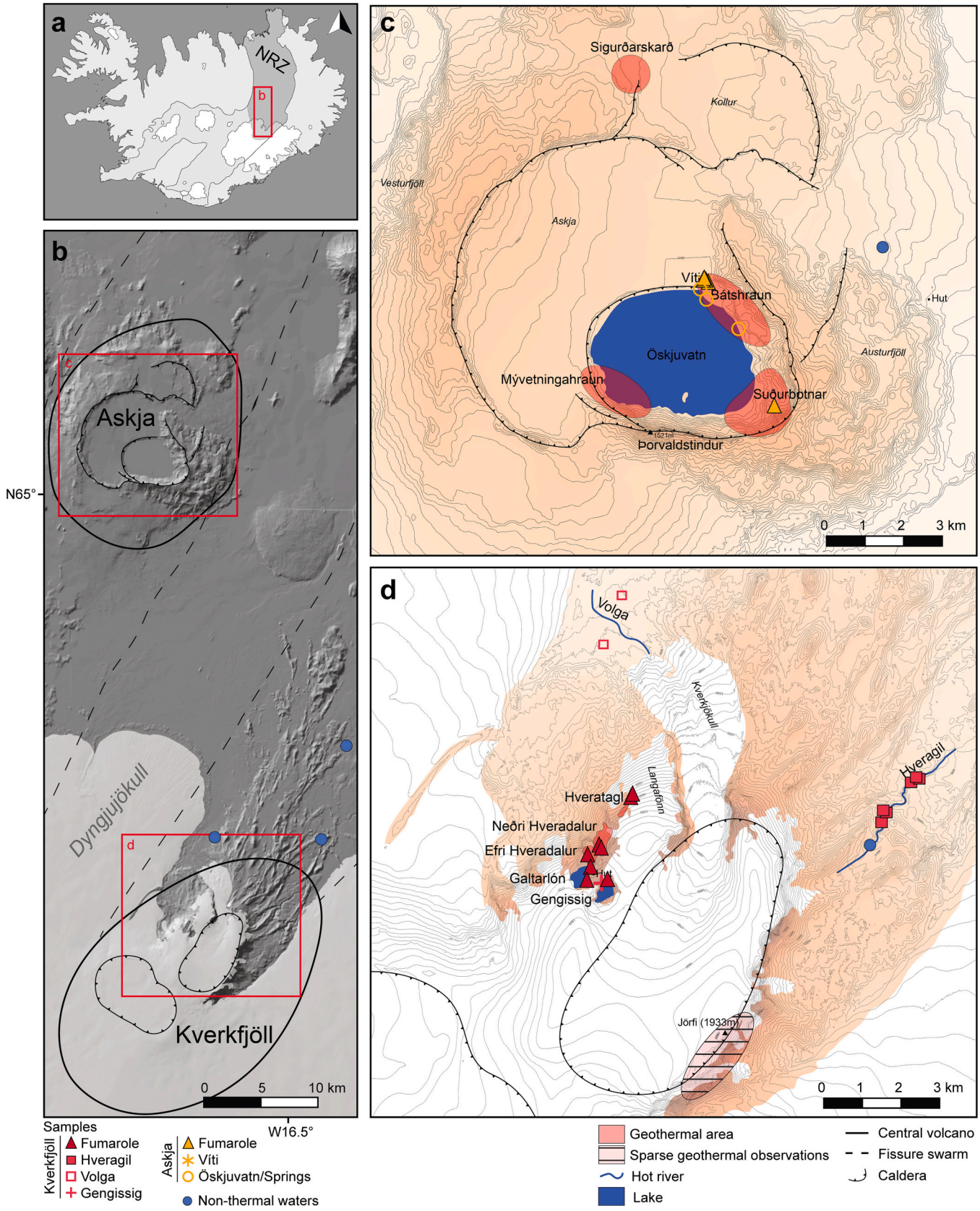


**Fig. 1.** (a,b) Map of Iceland, the Northern Rift Zone (NRZ) and study areas (red boxes). (c) The Askja central volcano and its four hydrothermally active areas. (d) The Kverkfjöll central volcano and hydrothermal manifestations: The Hveradalur hydrothermal area, two glacial lagoon, Galtarlón and Gengissig, and two thermal rivers Volga and Hveragil. Outlines of the hydrothermal areas and caldera faults are based on Jónasson and Einarsson (2009), Sigurgeirsson et al. (2015) and Oddsson (2016).

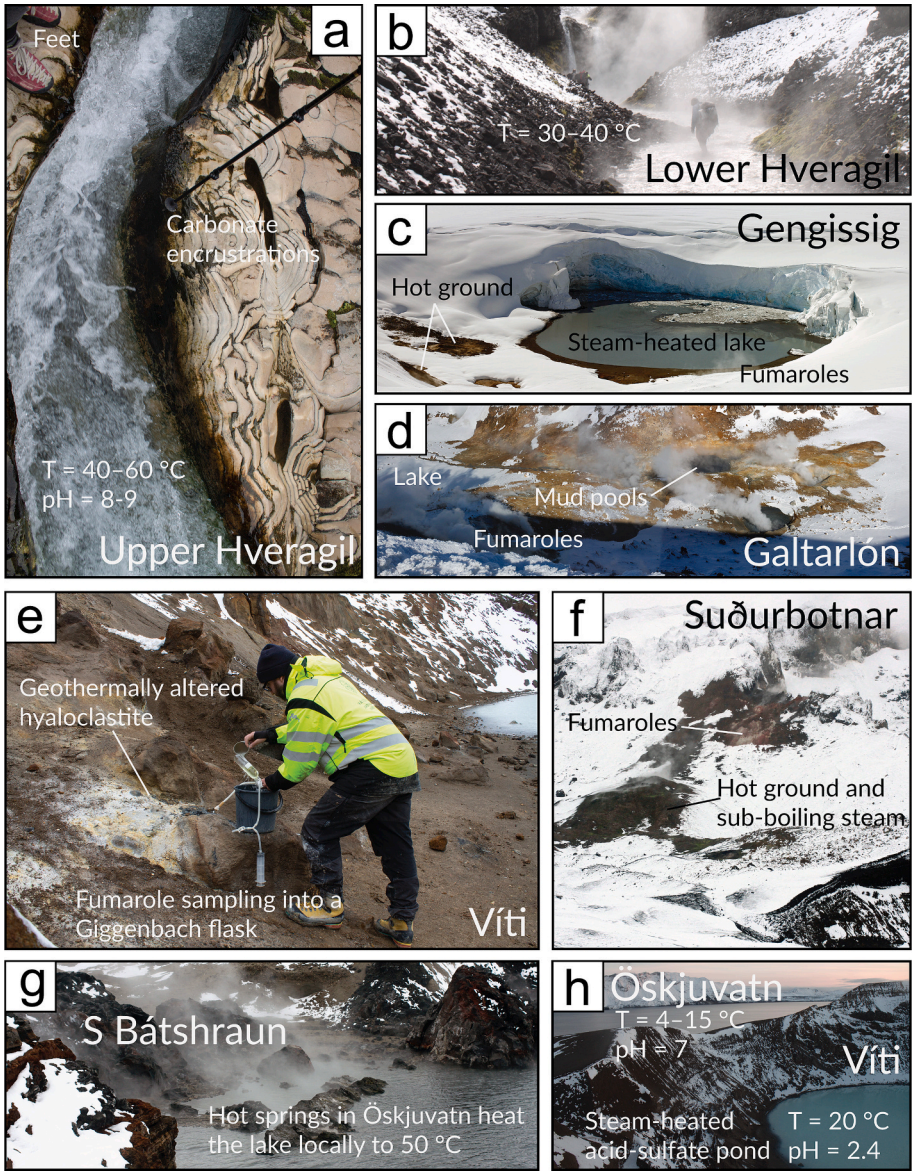


**Fig. 2.** Hydrothermal surface manifestations at Kverkfjöll and Askja. (a)-(b) Upper and lower portions of the Hveragil thermal river at Kverkfjöll. Hveragil water is mildly alkaline (pH = 8–9) with temperatures decreasing from $T = 60$ °C to T ≈ 30 °C from the upper to lower parts. (c)-(d) Gengissig and Galtarlón are steam-heated lakes located near the top of Hveradalur, at the edge of the Vatnajökull glacier. Vigorous boiling-point fumaroles and mud-pools typical of the Hveradalur area are seen in (d). (e) Fumarole sampling by the Víti pond at the Askja volcano. (f) Suðurbotnar thermal area in SE Askja. Hot grounds with sub-boiling steam, seen in the foreground, are typical in the easter margin of Lake Öskjuvatn. Several boiling-point fumaroles and high-T altered kaolonite-pyrite deposits are seen at higher altitude. (g) Bubbling hot springs are commonly found emanating from the floor of Lake Öskjuvatn, heating the lake water locally to >50 °C. (h) The Öskjuvatn crater lake and the Víti acid pond seen from the north.

non-thermal water samples were collected from Askja and Kverkfjöll during three field seasons between 2017 and 2019 (sample descriptions in Supplementary Table 1). All fumarole vapors were near to local boiling point temperatures (~94.5–96.5 °C at altitudes of 1050-1700 m). Thermal and non-thermal waters were filtered on-site through 0.2 μm mesh cellulose acetate filters and collected in polypropylene (PP) tubes that were washed three times with the sample. Sample splits for ICP-OES analysis were acidified on site to 1% $HNO_3$ (Merck Suprapur®). Total dissolved inorganic carbon ($\Sigma CO_2$) was analyzed using modified alkalinity titration (Stefansson et al., 2007) and the pH using a combination glass electrode. Major cation and Cl concentrations in water samples were determined by ICP-OES at the Institute of Earth Sciences (IES), University of Iceland.

Fumarole samples for major gas analysis were collected in evacuated borosilicate glass gas bulbs (100 to 350 mL) containing ~10–35 mL of 50% KOH solution (Fig. 3e). The concentrations of non-condensable gases ($H_2$, $N_2$, $O_2$, Ar, $CH_4$) were determined by gas chromatography at IES. Water concentrations were estimated gravimetrically. The $H_2S$ and $CO_2$ concentration in fumarole discharges were determined from the condensed vapor fraction by Hg-acetate titration and modified alkalinity titration, respectively (Arnórsson et al., 2006). Major gas and noble gas isotope data for 4 fumarole samples collected in 2017 have been published previously by Byrne et al. (2021).

### 3.2. Hydrogen and oxygen isotope sampling and analysis

Water and vapor condensate samples for hydrogen (δD-$H_2O$) and oxygen ($\delta^{18}O$-$H_2O$) isotope analysis were collected into PP vials. The δD-$H_2O$ and $\delta^{18}O$-$H_2O$ isotope ratios were determined by isotope ratio mass spectrometry (IRMS) at IES, performed on a Thermo Delta V Advantage continuous flow mass spectrometer, equipped with a Gasbench device. Data are reported in δ notation relative to VSMOW (Vienna Standard Mean Ocean Water) as δD and $\delta^{18}O$. Standard deviations of long-term repeat measurements are on average 0.7 ‰ and 0.05 ‰ for δD and $\delta^{18}O$, respectively (1σ).

### 3.3. Helium isotope sampling and analysis

Samples for noble gas analyses were taken from 8 fumaroles into copper tubes that were pre-flushed for at least ~15–30 min through a water lock and then sealed by cold-welding using screw clamps. Helium ($^3He$ and $^4He$) isotopes and $^{20}Ne$ were analyzed at the Woods Hole

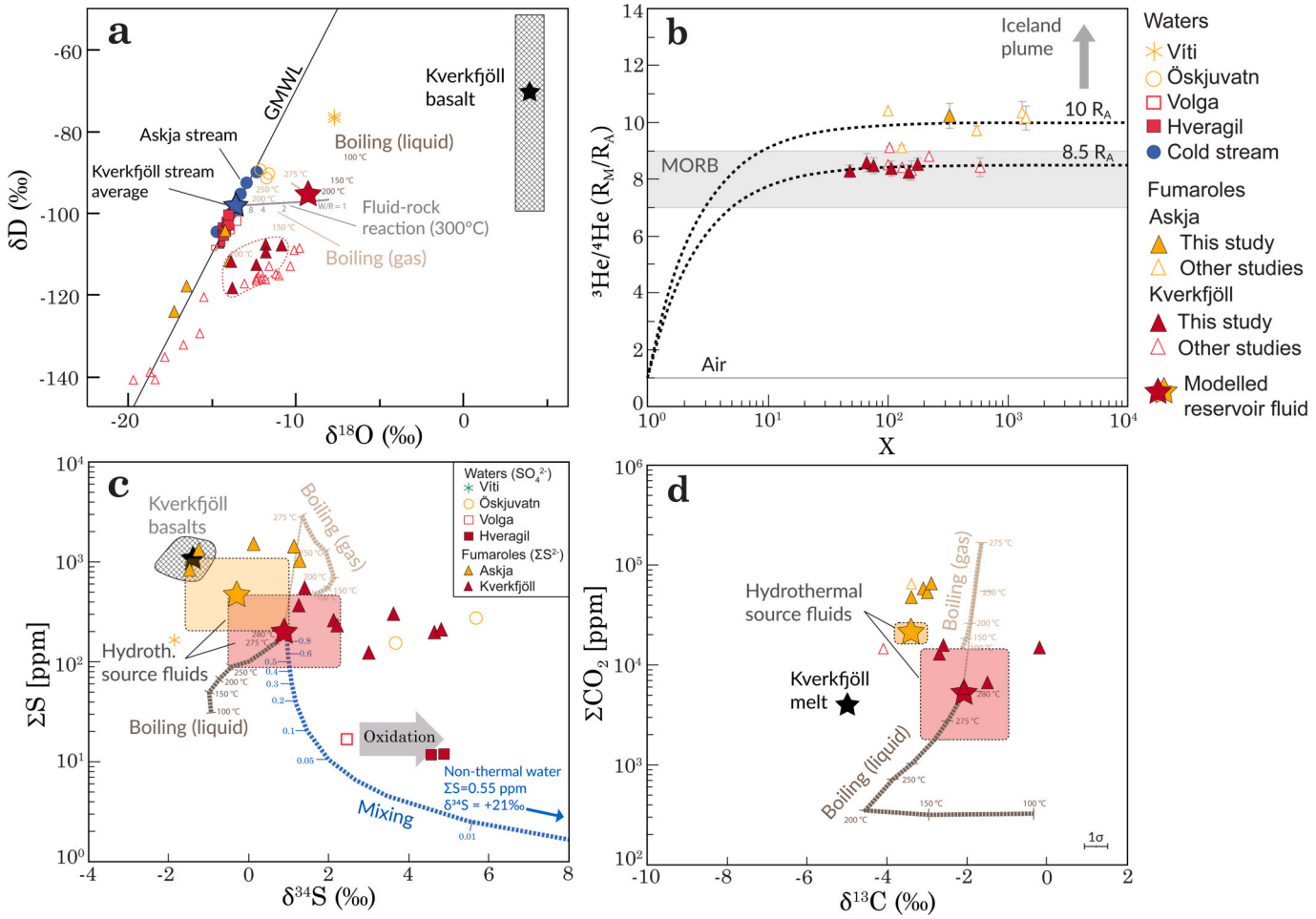


**Fig. 3.** Water, helium, sulfur and carbon isotope characteristics. (a) Water isotopes. Positive $\delta^{18}O$ shifts in the Kverkfjöll fumaroles indicate a reservoir that has experienced extensive fluid-rock interaction. Fluid-rock interaction of meteoric water with basalt at 300 °C (grey curve) was simulated using PHREEQC, Parkhurst and Appelo (1999) and available mineral-water isotope fractionation factors (Kleine et al., 2020, Supplementary Information) (b) Measured $^3He/^4He$ versus the X-factor (i.e., $^4He/^{20}Ne$ normalized to air). Mixing lines are shown for mixing between air and components with $^3He/^4He$ of 10 $R_A$ and 8.5 $R_A$, corresponding to the average $^3He/^4He$ signatures of Askja and Kverkfjöll signatures, respectively. The X factor is used to quantify air contamination in the sample, and is calculated as $X = \left[\frac{4He}{20Ne}\right]_{sample} / \left[\frac{4He}{20Ne}\right]_{air}$ (e.g., Hilton, 1996). All samples have high X values (>>10), signaling minimal air contamination. Kverkfjöll samples plot within the mid-ocean ridge basalt (MORB) field (8 ± 1 RA; Graham, 2002), whereas higher $^3He/^4He$ at Askja suggest a component derived from the high-$^3He/^4He$ component of the Iceland plume (>30 $R_A$, Harðardóttir et al., 2018). (c) ΣS versus $\delta^{34}S$ in $H_2S$(g) and $SO_4$(lq). The $\delta^{34}S$-$H_2S$ values of the Askja fumaroles are consistent with a magmatic gas source for S. The positive $\delta^{34}S$-$SO_4$ of hot springs is compatible with oxidation of $\Sigma S^{2-}$ from a one-phase reservoir (Hveragil) liquid or fumarolic $H_2S$ (Lake Öskjuvatn). Mixing line between the estimated Kverkfjöll reservoir liquid composition and meteoric water (Stefánsson et al., 2015) is shown with a blue dashed line. (d) $\Sigma CO_2$ versus $\delta^{13}C$. Model curves for depressurization boiling are shown for both liquid (tan) and vapor (dark brown) phases in (a), (c) and (d). Analytical uncertainties (1σ) are smaller than the sizes of the symbols except for $^3He/^4He$. Red and green stars and boxes indicate the average values and variation of modelled reservoir fluid compositions of Kverkfjöll and Askja, respectively. (For interpretation of the references to colour in this figure legend, the reader is referred to the web version of this article.)

Oceanographic Institute, US, following methods outlined in Barry et al. (2022). The helium isotope ratios ($^3He/^4He$) are reported relative to the atmospheric ratio ($R_a = 1.4 \times 10^{-6}$) and corrected for air contamination using $^4He/^{20}Ne$ (Hilton, 1996). The measured $^4He/^{20}Ne$ (15–344, or X = 48–1415, where X is the air-normalized $^4He/^{20}Ne$ ratio (Hilton, 1996)) result in only minor $^3He/^4He$ corrections (0.00 to 0.12 $R_a$) indicating that the samples are relatively unaffected by air-contamination. The estimated instrumental uncertainty (2σ) is between 0.22 and 0.44 $R_a$.

### 3.4. Carbon isotope sampling and analysis

Samples for $\delta^{13}C$-$CO_2$ analysis were collected as dry-gas or as steam condensate in alkali solutions. The $\delta^{13}C$-$CO_2$ composition in dry-gas samples was measured at the Goethe University Frankfurt, Germany, with a Flash EA 1112 (Thermo) linked to the continuous flow system of a ThermoFischer MAT 253 IRMS, according to the protocol provided by Fiebig et al. (2004, 2007). The estimated analytical uncertainty (1σ) is ±0.2‰. The $\delta^{13}C$-$CO_2$ compositions in alkali vapor condensates were analyzed at IES using Cavity ring-down spectrometers of a Picarro G G2201-I isotope analyzer, equipped with a Automate FX sample preparation device for $CO_2$ extraction form the samples. The estimated analytical uncertainty (1σ) is ±0.3‰. Data are reported in δ notation relative to the Vienna Pee Dee Belemnite (VPDB).

### 3.5. Sulfur isotope sampling and analysis

Sulfate ($SO_4$) in 6 water samples was precipitated as $BaSO_4$(s) by adding excess 1 M $BaCl_2$ solution to a sample aliquot. The sample was then filtered through a 0.2 μm cellulose acetate filter and the $BaSO_4$ precipitate collected from the filter paper in deionized water, and dried. Analogously, sulfide ($H_2S$) in 14 fumarole gases was precipitated as ZnS

(s) by adding excess 1 M Zn-acetate solution to the gas condensates. The gas condensate containing ZnS(s) was then filtered, and ZnS(s) precipitate was collected and dried. The resulting $BaSO_4$(s) and ZnS(s) precipitates were dissolved, purified and extracted as $Ag_2S$(s) using "Thode" (Thode et al., 1961) and HCl extraction protocols (Alt and Shanks III, 1998), respectively, with modifications described in Gunnarsson-Robin et al. (2017).

All three stable sulfur isotope ratios ($^{33}S/^{32}S$, $^{34}S/^{32}S$, $^{36}S/^{32}S$) were determined by gas source dual-inlet IRMS using a Thermo Scientific MAT 253 at the Stable Isotope Geobiology Laboratory at the Massachusetts Institute of Technology using an analytical setup detailed by Ono et al. (2007, 2012) and Gunnarsson-Robin et al. (2017). In short, $Ag_2S$(s) is first fluorinated at ~300 °C for >6 h, resulting in a full conversion of S to $SF_6$(g), which then passes a series of in-line cryogenic traps and a chromatographic purification step before introduction to the mass spectrometer. The samples were analyzed during the same sessions as data reported in Ranta et al. (2022). The $^{34}S/^{32}S$ data are reported in standard δ notation relative to V-CDT (Vienna Canyon Diablo Troilite). The $^{33}S/^{32}S$ and $^{36}S/^{32}S$ data are reported as $\Delta^{33}S$ and $\Delta^{36}S$, defined as

$$\Delta^{x}S = ln(\delta^{x}S + 1) - \theta^{x} ln(\delta^{34}S + 1) \quad (1)$$

where $\Delta^{x}$ denotes the deviation of $\delta^{x}S$ from a mass-dependent fractionation line, where x = 33 or 36, and $\theta^{33} = 0.515$ and $\theta^{36} = 1.90$. Because the IAEA-S-1 lacks reference values for $\Delta^{33}S$ and $\Delta^{36}S$, they are anchored to the CDT scale using replicate measurements of the IAEA-S-1 reference material and average literature values of IAEA-S-1 vs. CDT. We use IAEA-S-1 $\Delta^{33}S_{CDT}$ and $\Delta^{36}S_{CDT}$ values of of +0.109 and − 0.730‰, respectively (Ranta et al., 2022). Repeat measurements of IAEA-S-1 yield respective $\delta^{34}S$, $\Delta^{33}S$ and $\Delta^{36}S$ values of −1.19±0.17‰, +0.100 ±0.004‰ and −0.669±0.068‰, relative to the MIT reference gas SG1. The analytical uncertainties are 0.12, 0.004, and 0.086 ‰ (all 1σ) for $\delta^{34}S$, $\Delta^{33}S$ and $\Delta^{36}S$, respectively, based on the long-term reproducibility of an in-house $Ag_2S$ (Sigma Aldrich) standard.

**Table 1**
Chemical and isotope compostion of water samples.

| Sample ID | Location | Type[a] | Latitude (N) | Longitude (W) | T | pH | $SiO_2$ | B | Na | K | Ca | Mg | Fe |
|---|---|---|---|---|---|---|---|---|---|---|---|---|---|
| | | | | | °C | | ppm | ppm | ppm | ppm | ppm | ppm | ppm |
| *Kverkfjöll* | | | | | | | | | | | | | |
| 18-ER/KVK-01 | Kreppa tributary | cs | 64°42.576' | 016°28.952' | 5 | 7.54 | 8.15 | b.d. | 1.82 | 0.25 | 2.55 | 1.15 | 0.008 |
| 18-ER/KVK-02 | Hveragil | tr | 64°41.589' | 016°30.756' | 35 | 8.90 | 113 | 0.176 | 182 | 15.9 | 15.2 | 26.5 | b.d. |
| 18-ER/KVK-03 | Hveragil | tr | 64°41.642' | 016°30.661' | 22 | 8.10 | 50.3 | 0.080 | 97.6 | 6.57 | 12.9 | 22.6 | b.d. |
| 18-ER/KVK-04 | Hveragil | tr | 64°41.619' | 016°30.675' | 19 | 8.01 | 43.9 | 0.067 | 84.7 | 5.71 | 12.7 | 20.5 | b.d. |
| 18-ER/KVK-05 | Lindaá | cs | 64°48.319' | 016°22.314' | 3 | 8.49 | 16.2 | 0.022 | 19.8 | 0.97 | 5.10 | 5.04 | b.d. |
| 18-ER/KVK-06 | Sigurðarskáli | cs | 64°44.812' | 016°37.963' | 6 | 7.18 | 9.46 | b.d. | 4.12 | 0.38 | 8.11 | 2.23 | 0.006 |
| 18-ER/KVK-07 | Volga | tr | 64°44.135' | 016°40.125' | 20 | 7.76 | 96.1 | 0.661 | 93.6 | 9.46 | 22.8 | 11.2 | 0.011 |
| 18-ER/KVK-08 | Hveragil | tr | 64°41.158' | 016°31.684' | 35 | 8.54 | 96.4 | 0.184 | 199 | 15.2 | 10.9 | 27.6 | 0.030 |
| 18-ER/KVK-09 | Hveragil | tr | 64°41.149' | 016°31.623' | 44 | 8.57 | 130 | 0.201 | 204 | 18.4 | 17.9 | 28.2 | b.d. |
| 18-ER/KVK-10 | Arnardalsá | cs | 65°07.473' | 015°58.036' | 3 | 8.94 | 16.9 | 0.015 | 12.2 | 0.41 | 4.81 | 1.49 | 0.024 |
| 19-EM-KVK-1 | Hveragil | tr | 64°41.080' | 016°31.698' | 48 | 8.45 | 132 | 0.190 | 202 | 19.7 | 18.1 | 27.9 | 0.008 |
| 19-ER/KVK-07 | Gengissig | s | 64°40.187' | 016°41.177' | 10 | 6.64 | 59.0 | 0.070 | 14.5 | 2.89 | 42.1 | 5.24 | b.d. |
| 19-ER/KVK-08 | Hveragil, upper | cs | 64°40.705' | 016°32.158' | 2 | 7.83 | 6.90 | b.d. | 5.66 | 0.30 | 8.12 | 1.73 | 0.031 |
| 19-ER/KVK-10 | Volga | tr | 64°43.318' | 016°40.933' | 26 | 7.79 | 110 | 0.744 | 106 | 11.5 | 23.0 | 10.6 | 0.025 |
| *Askja* | | | | | | | | | | | | | |
| 18-ER/ASK-05 | Öskjuvatn | l | 65°02.722' | 016°43.515' | 13 | 6.96 | 93.6 | 0.352 | 130 | 6.65 | 108 | 29.5 | 0.281 |
| 18-ER/ASK-06 | Öskjuvatn | ts | 65°02.738' | 016°43.545' | 52 | 6.41 | 142 | 0.576 | 205 | 10.4 | 336 | 81.9 | 2.46 |
| 18-ER/ASK-07 | Víti | ts | 65°02.787' | 016°43.520' | 20 | 2.43 | 156 | 0.090 | 12.0 | 3.55 | 46.0 | 19.8 | 29.5 |
| 18-ER/ASK-08 | Víti | ts | 65°02.817' | 016°43.590' | 20 | 2.45 | 155 | 0.084 | 8.43 | 1.75 | 43.0 | 18.9 | 28.9 |
| 18-ER/ASK-09 | NE Askja caldera | cs | 65°03.345' | 016°37.575' | 1 | 7.68 | 14.2 | 0.014 | 8.38 | 0.35 | 10.5 | 2.49 | 0.294 |
| 19-ER/ASK-01 | Öskjuvatn | ts | 65°02.173' | 016°42.295' | 50 | 7.86 | 153 | 0.077 | 113 | 6.43 | 44.3 | 11.7 | 0.018 |
| 19-ER/Jök-01 | Jökulsaá-á-Fjöllum | cs | 65°00.850' | 016°15.055' | 6 | 8.08 | 17.0 | 2.74 | 15.8 | 0.83 | 13.9 | 4.36 | 0.120 |

| Sample ID | Al | F | Cl | $\Sigma CO_2$ | $SO_4$ | $\delta D\text{-}H_2O$ | $\delta^{18}O\text{-}H_2O$ | $\delta^{34}S_{V\text{-}CDT}\text{-}SO_4$ | | $\Delta^{33}S_{CDT}\text{-}SO_4$ | | $\Delta^{36}S_{CDT}\text{-}SO_4$ | |
|---|---|---|---|---|---|---|---|---|---|---|---|---|---|
| | ppm | ppm | ppm | ppm | ppm | ‰ | ‰ | ‰ | | ‰ | | ‰ | |
| *Kverkfjöll* | | | | | | | | | | | | | |
| 18-ER/KVK-01 | 0.028 | 0.04 | 0.78 | 37.0 | 0.87 | −99.3 | −13.63 | | | | | | |
| 18-ER/KVK-02 | 0.023 | 0.77 | 35.3 | 570 | 32.9 | −104.1 | −14.19 | | | | | | |
| 18-ER/KVK-03 | 0.017 | 0.48 | 13.7 | 253 | 19.8 | −102.2 | −14.10 | | | | | | |
| 18-ER/KVK-04 | 0.018 | 0.42 | 11.5 | 229 | 17.4 | −100.4 | −14.01 | | | | | | |
| 18-ER/KVK-05 | 0.024 | 0.15 | 3.74 | 53.0 | 6.24 | −100.1 | −13.91 | | | | | | |
| 18-ER/KVK-06 | 0.025 | 0.08 | 0.55 | 23.0 | 10.1 | −99.5 | −13.62 | | | | | | |
| 18-ER/KVK-07 | 0.049 | 0.51 | 52.7 | 165 | 50.4 | −103.8 | −13.96 | 2.46 | ±0.12 | −0.003 | ±0.014 | 0.049 | ±0.041 |
| 18-ER/KVK-08 | 0.068 | 0.76 | 33.8 | 399 | 43.7 | −102.8 | −14.03 | | | | | | |
| 18-ER/KVK-09 | 0.046 | 0.85 | 40.7 | 431 | 35.8 | −105.4 | −14.32 | 4.89 | ±0.12 | −0.007 | ±0.007 | 0.062 | ±0.054 |
| 18-ER/KVK-10 | 0.084 | 0.13 | 1.78 | 34.0 | 2.0 | −89.9 | −12.34 | | | | | | |
| 19-EM-KVK-1 | 0.009 | | 39.4 | 384 | 35.2 | −103.6 | −14.34 | 4.57 | ±0.12 | 0.004 | ±0.014 | 0.023 | ±0.025 |
| 19-ER/KVK-07 | b.d. | | b.d. | 68.0 | 103 | −99.5 | −13.27 | | | | | | |
| 19-ER/KVK-08 | 0.039 | | b.d. | 39.0 | 1.11 | −95.2 | −13.30 | | | | | | |
| 19-ER/KVK-10 | 0.015 | | 60.5 | 180 | 49.7 | −101.8 | −13.56 | | | | | | |
| *Askja* | | | | | | | | | | | | | |
| 18-ER/ASK-05 | 13.5 | 0.53 | 46.5 | 163 | 462 | −90.2 | −11.62 | 3.68 | ±0.12 | −0.010 | ±0.025 | 0.042 | ±0.090 |
| 18-ER/ASK-06 | 13.6 | 0.06 | 141 | 628 | 822 | −91.2 | −11.77 | 5.69 | ±0.12 | 0.015 | ±0.010 | 0.011 | ±0.063 |
| 18-ER/ASK-07 | 13.5 | 0.02 | 4.70 | b.d. | 492 | −76.2 | −7.71 | | | | | | |
| 18-ER/ASK-08 | 13.7 | 0.02 | 1.59 | b.d. | 496 | −76.8 | −7.69 | −1.85 | ±0.12 | 0.020 | ±0.006 | −0.116 | ±0.073 |
| 18-ER/ASK-09 | 0.160 | 0.10 | 1.33 | 34.0 | 17.9 | −92.5 | −12.94 | | | | | | |
| 19-ER/ASK-01 | 0.025 | | 4.57 | 221 | 142 | −89.15 | −12.1 | | | | | | |
| 19-ER/Jök-01 | 0.114 | | b.d. | 64.0 | 11.6 | −104.50 | −14.7 | | | | | | |

b.d. = below detection.
[a] cs = cold stream or river; tr = thermal river; l = lake; ts = thermal spring.

## 4. Results

### 4.1. Water compositions

The chemical compositions of non-thermal and thermal waters are reported in Table 1 and Figs. S1-S3. The non-thermal waters collected at both localities are characterized by low total dissolved solid concentrations (TDS; 53–130 ppm) and low total dissolved carbon ($\Sigma CO_2$ = 23–53 ppm) and $SO_4$ (0.9–18 ppm) content (Fig. S2a).

At Kverkfjöll, the thermal Hveragil river water has low $SO_4$ contents (17–44 ppm) coupled to high $\Sigma CO_2$ content (up to 580 ppm), neutral to alkaline pH values (7.2–8.9) and moderate temperatures (18.7–61.5 °C; Fig. S2a). The B, Cl, $SiO_2$ (Fig. S1) and $\Sigma CO_2$ concentrations of the Hveragil all show a positive linear correlation with temperature.

At Askja, the Lake Öskjuvatn water has low temperature ($T$ = 12.5 °C), close to neutral pH (7.0), and elevated $SO_4$ content (460 ppm) and relatively high concentrations of $\Sigma CO_2$ (163 ppm), $SiO_2$ (94 ppm) and Cl (46 ppm). The Víti crater lake water is warm ($T$ = 20 °C) and acidic (pH = 2.5), with low concentrations of $\Sigma CO_2$ (below detection limit) and Cl (1.6–4.7 ppm), but high concentrations of $SO_4$ (490 ppm) and $SiO_2$ (155 ppm). A circumneutral hot spring (pH = 6.4, $T$ = 52 °C) on the outer southern rim of the Víti crater was found to have anomalous high concentrations of $\Sigma CO_2$ (628 ppm), $SO_4$ (822 ppm), Cl (141 ppm) and $SiO_2$ (142 ppm).

### 4.2. Fumarole compositions

The vapor compositions of fumarole discharges at Kverkfjöll and Askja are reported in Table 2 and shown in Figs. S2 and S3 together with previously published data (Poreda et al., 1992; Ólafsson et al., 2000; Byrne et al., 2021; Stefánsson, 2017). The fumarole discharges at Kverkfjöll are dominated by water ($H_2O$ = 98.3–99.7 mol%), which is typical for Icelandic fumaroles (Stefánsson, 2017), followed by $CO_2$ (2450–15,510 μmol/mol) and $H_2S$ (94–631 μmol/mol; Fig. S2c). The $CH_4$ concentrations at Kverkfjöll (1.6–15.0 μmol/mol) are generally higher than at Askja at (0.9–3.6 μmol/mol; Fig. S2d). The fumarole discharge at Askja has lower water content ($H_2O$ = 96.7–98.0 mol%) compared to most other Icelandic hydrothermal areas (Stefánsson, 2017), followed by $CO_2$ (18650–31,980 μmol/mol) and $H_2S$ (790–1770 μmol/mol). A fumarole sample from Suðurbotnar has an anomalous composition, with $H_2S$ concentrations below detection and high $CH_4$ (10 μmol/mol). No significant temporal changes are observed in the available vapor major gas data from Kverkfjöll and Askja from 1983 to present (Poreda et al., 1992; Ólafsson et al., 2000).

### 4.3. Hydrogen and oxygen isotopes

Non-thermal stream waters in the Kverkfjöll area ($n$ = 4) have δD values between −100.1 and −95.2 ‰ and $\delta^{18}O$ values between −13.9 and −13.3 ‰, falling approximately on the Global Meteoric Water Line (GMWL; $\delta D = 8 \times \delta^{18}O + 10$; Fig. 3a, Table 1). These values agree well with the local precipitation in the central highlands (Árnason, 1976). The thermal Hveragil water records δD and $\delta^{18}O$ values extending from local non-thermal waters down to lower values of −107.8% and −14.5 ‰, respectively. The Kverkfjöll fumaroles record some of the lowest δD and $\delta^{18}O$ values in Iceland, with fumarole vapors from Hveratagl showing values as low as −140.8 and −19.7 ‰ (Ólafsson et al., 2000; Fig. 3a). Kverkfjöll fumaroles with higher δD and $\delta^{18}O$ values (up to −108 ‰ and −10 ‰, respectively) tend to have positive $\Delta^{18}O$ (difference in $\delta^{18}O$ between the sample and GMWL at a given δD value).

Local melt water stream at Askja has δD and $\delta^{18}O$ values of −92.5 and −12.9 ‰, respectively, reflecting the local precipitation (Árnason, 1976). Near-shore samples taken from lake Öskjuvatn have higher δD and $\delta^{18}O$ values and display minor positive $\Delta^{18}O$ relative to GMWL. The highest δD, $\delta^{18}O$ and $\Delta^{18}O$ values at Askja are recorded from Víti at −76.2 ‰, −7.7 ‰ and +3 ‰, respectively. Compared to the thermal and non-thermal waters, the Askja fumaroles have more negative δD (between −124 and −104 ‰) and $\delta^{18}O$ (−17.3 to −14.0 ‰), and plot close to the GMWL.

### 4.4. Helium isotopes

Fumarole vapor helium isotope ($^3He/^4He$) compositions from Kverkfjöll and Askja are reported in Table 2 and Fig. 3b and S5 together with previously reported data (Poreda et al., 1992; Füri et al., 2010; Byrne et al., 2021). The air-corrected $^3He/^4He$ are 8.28–8.70 $R_c/R_A$ for Kverkfjöll and 10.15–10.33 $R_c/R_A$ for Askja (this study, Byrne et al., 2021). These recent values agree within error with $^3He/^4He$ values of 8.54–8.84 $R_a$ (Kverkfjöll) and 10.45 $R_a$ (Askja) measured about 30 years prior by Poreda et al. (1992), and 8.43–9.14 $R_a$ (Kverkfjöll) and 9.08–9.70 $R_a$ (Askja) measured about 10 years prior by Füri et al. (2010). Generally, the $^3He/^4He$ measured in fumaroles and hot springs at Kverkfjöll and Askja are similar to $^3He/^4He$ measured in olivine crystals and basaltic glasses least affected by degassing in Pleistocene lavas from the two volcanoes (Macpherson and Mattey, 1994; Harðardóttir et al., 2018).

### 4.5. Carbon isotopes

The $\delta^{13}C\text{-}CO_2$ composition from Kverkfjöll and Askja are reported in Table 2 and Fig. 3d. The values obtained here of −0.2 to −2.7 ‰ for Kverkfjöll and − 2.9 to −3.4 ‰ for Askja are similar but slightly less negative than published fumarole $\delta^{13}C\text{-}CO_2$ data of −2.0 to −4.1 ‰ for Kverkfjöll and −3.4 to −4.2 ‰ for Askja (Poreda et al., 1992; Barry et al., 2014).

### 4.6. Sulfur isotopes

The multiple sulfur isotope compositions ($\delta^{34}S$ and $\Delta^{33}S$) of $H_2S$ from 12 fumaroles and $SO_4$ for 5 thermal waters are reported in Tables 1 and 2 and Fig. 3c. The $\delta^{34}S\text{-}H_2S$ values in fumaroles from Kverkfjöll (+1.14 to +4.82 ‰) are more positive relative to Askja (−1.47 to +1.28 ‰; Fig. 3c). The $\Delta^{33}S\text{-}H_2S$ values of the Kverkfjöll and Askja fumaroles show a similar range of (−0.031 to +0.003 ‰). The thermal waters have $\delta^{34}S\text{-}SO_4$ values ranging from −1.85 to +5.69 ‰ and $\Delta^{33}S\text{-}SO_4$ values from −0.010 to +0.020 ‰.

The range of $\delta^{34}S$ values at Askja is typical of meteoric water-fed VHSs in Iceland such as Kerlingarfjöll, Geysir and Krafla (Stefánsson et al., 2015; Gunnarsson-Robin et al., 2017), whereas the $\delta^{34}S$ values of the Kverkfjöll fumaroles are more positive. The $\Delta^{33}S$ compositions of Kverkfjöll and Askja fumaroles and thermal waters are similar to those previously reported from hydrothermal wells, fumaroles and hot springs from meteoric water-fed VHSs in Iceland (Stefánsson et al., 2015; Gunnarsson-Robin et al., 2017, 2020), and indistinguishable from the $\Delta^{33}S$ range of Icelandic basalts (−0.045 to +0.016; Ranta et al., 2022).

## 5. Discussion

Our aim in the discussion is to determine the volatile contribution of intrusive magmatic degassing into hydrothermal fluids in Iceland. First, we estimate the isotopic and elemental source fluid compositions of Askja and Kverkfjöll by modelling the effects of shallow hydrothermal processes on the chemistry of surface fluids (5.1). Second, we approximate the isotopic and elemental compositions of magmatic gases by employing volatile solubility models that simulate degassing of ascending basaltic intrusions (5.2). Then, we compare the modelling results to evaluate whether chemical fingerprints of magmatic gases are present in the hydrothermal fluids (5.3). Finally, we use volatile flux calculations to assess, in terms of mass balance, whether and what types of magmatic degassing are the most plausible sources of magmatic volatiles in hydrothermal systems of Iceland (5.4 and 5.5).

**Table 2**
Chemical and isotope compostion of fumarole vapor.

| Sample | Location | Latitude (N) | Longitude (W) | $H_2O$ | $CO_2$ | $H_2S$ | $H_2$ | $O_2$ | $N_2$ | Ar | $CH_4$ |
|---|---|---|---|---|---|---|---|---|---|---|---|
| | | | | μmol/mol | μmol/mol | μmol/mol | μmol/mol | μmol/mol | μmol/mol | μmol/mol | μmol/mol |
| *Kverkfjöll* | | | | | | | | | | | |
| 19-ER/KVK-01 | Efri Hveradalur | 64°40′21.2” | 016°41′35.6” | 996,605 | 2799 | 237 | 338 | 0.56 | 16 | 0.2 | 3.9 |
| 19-ER/KVK-02 | Efri Hveradalur | 64°40′16.1” | 016°41′38.2” | 993,266 | 6294 | 224 | 156 | 1.40 | 49 | 1.2 | 8.4 |
| 19-ER/KVK-03 | Efri Hveradalur | 64°40′36.8” | 016°41′17.3” | 994,031 | 5431 | 262 | 226 | 0.44 | 36 | 0.9 | 12.2 |
| 19-ER/KVK-04 | Neðri Hveradalur | 64°40′38.7” | 016°41′19.5” | 994,778 | 4482 | 293 | 340 | 0.80 | 94 | 1.3 | 9.0 |
| 19-ER/KVK-05 | Galtarlón | 64°40′30.5” | 016°41′32.9” | 996,823 | 2453 | 414 | 51 | 8.90 | 243 | 3.3 | 4.8 |
| 19-ER/KVK-06 | Gengissig | 64°40′15.4” | 016°41′04.7” | 993,023 | 6649 | 140 | 148 | 0.58 | 30 | 0.5 | 10.2 |
| 17-KVE-01[a] | Hveratagl | | | 987,143 | 11,331 | 345 | 687 | 1.02 | 478 | 7.2 | 7.7 |
| 17-KVE-02[a] | Hveratagl | | | 983,415 | 15,506 | 631 | 374 | 0.97 | 59 | 1.2 | 12.0 |
| 17-KVE-03[a] | Hveratagl | | | | | | | | | | |
| *Askja* | | | | | | | | | | | |
| 17-ASK-01[a] | Víti | | | 980,054 | 18,653 | 963 | 250 | 0.43 | 70 | 8.9 | 2.4 |
| 17-ASK-02[a] | Víti | | | 979,968 | 18,673 | 794 | 522 | 1.63 | 39 | 0.9 | 0.97 |
| 18-ER/ASK-01 | Víti | 65°02′49.5” | 016°43′26.8” | 977,123 | 20,538 | 1654 | 635 | 0.84 | 47 | 1.0 | 0.90 |
| 18-ER/ASK-02 | Víti | 65°02′49.2” | 016°43′26.6” | 974,911 | 23,091 | 1195 | 514 | 5.15 | 277 | 4.7 | 1.46 |
| 18-ER/ASK-03 | Víti | 65°02′49.0” | 016°43′25.6” | 969,275 | 28,619 | 1769 | 160 | 3.43 | 166 | 4.2 | 3.59 |
| 18-ER/ASK-04 | Víti | 65°02′47.2” | 016°43′28.8” | 973,050 | 25,319 | 1541 | 8 | 0.35 | 78 | 2.1 | 1.14 |
| 19-ER/ASK-02 | Suðurbotnar | 65°00′57.7” | 016°40′56.0” | 967,167 | 31,982 | b.d. | 282 | 20 | 530 | 8.0 | 10.0 |

| Sample | $\delta^{18}O$-$H_2O$ | $^4He$ | $^3He/^4He$ | | $^3He/^4He$ | $^4He/^{20}Ne$ | X[d] | $\delta^{13}C$-$CO_2$ | | $\delta^{34}S_{V\text{-}CDT}$-$H_2S$ | | $\Delta^{33}S_{CDT}$-$H_2S$ | | $\Delta^{36}S_{CDT}$-$H_2S$ | |
|---|---|---|---|---|---|---|---|---|---|---|---|---|---|---|---|
| | ‰ | $cm^3STP/cm^3$ ($x10^{-7}$) | $R_M/R_A$[b] | | $R_C/R_A$[c] | | | ‰ | | ‰ | | ‰ | | ‰ | |
| *Kverkfjöll* | | | | | | | | | | | | | | | |
| 19-ER/KVK-01 | −10.85 | 11.6 | 8.47 | ±0.28 | 8.57 | 24.10 | 75.6 | −1.5 | ±0.2 | 4.82 | ±0.12 | −0.031 | ±0.013 | 0.280 | ±0.111 |
| 19-ER/KVK-02 | −11.80 | 8.2 | 8.28 | ±0.22 | 8.43 | 15.30 | 48.0 | −0.2 | ±0.2 | 4.65 | ±0.12 | −0.013 | ±0.013 | 0.206 | ±0.073 |
| 19-ER/KVK-03 | −12.36 | 20.6 | 8.37 | ±0.27 | 8.44 | 33.92 | 106 | −2.7 | ±0.3 | 2.22 | ±0.12 | −0.005 | ±0.005 | 0.157 | ±0.036 |
| 19-ER/KVK-04 | −13.79 | 21.8 | 8.52 | ±0.22 | 8.56 | 56.30 | 177 | | | 2.13 | ±0.12 | −0.012 | ±0.010 | 0.205 | ±0.067 |
| 19-ER/KVK-05 | −11.79 | 8.6 | 8.58 | ±0.32 | 8.70 | 21.11 | 66.3 | −2.1 | ±0.3 | 1.26 | ±0.12 | 0.003 | ±0.007 | 0.164 | ±0.054 |
| 19-ER/KVK-06 | −13.95 | 23.1 | 8.24 | ±0.27 | 8.28 | 47.51 | 149 | −2.6 | ±0.3 | 3.01 | ±0.12 | −0.012 | ±0.012 | 0.133 | ±0.059 |
| 17-KVE-01[a] | | 126.0 | 8.30 | ±0.34 | 8.35 | 37.70 | 157 | | | 3.63 | ±0.12 | −0.015 | ±0.011 | 0.225 | ±0.034 |
| 17-KVE-02[a] | | 112.0 | 8.42 | ±0.33 | 8.44 | 142.5 | 587 | | | 1.41 | ±0.12 | −0.008 | ±0.005 | 0.043 | ±0.067 |
| 17-KVE-03[a] | | | | | | | | | | 1.14 | ±0.12 | −0.001 | ±0.017 | 0.058 | ±0.031 |
| *Askja* | | | | | | | | | | | | | | | |
| 17-ASK-01[a] | | 47.1 | 10.33 | ±0.40 | 10.33 | 318.2 | 1316 | | | −1.47 | ±0.12 | −0.002 | ±0.007 | 0.049 | ±0.064 |
| 17-ASK-02[a] | | 43.3 | 10.15 | ±0.42 | 10.15 | 343.7 | 1415 | | | | | | | | |
| 18-ER/ASK-01 | −14.22 | 15.49 | 10.23 | ±0.44 | 10.26 | 103.8 | 326 | −3.4 | ±0.3 | 1.14 | ±0.12 | −0.012 | ±0.014 | 0.032 | ±0.076 |
| 18-ER/ASK-02 | −17.26 | | | | | | | −3.0 | ±0.3 | 1.28 | ±0.12 | −0.017 | ±0.008 | 0.243 | ±0.064 |
| 18-ER/ASK-03 | −16.52 | | | | | | | −2.9 | ±0.3 | 0.13 | ±0.12 | −0.012 | ±0.009 | 0.075 | ±0.046 |
| 18-ER/ASK-04 | −13.96 | | | | | | | −3.1 | ±0.3 | −1.24 | ±0.12 | 0.002 | ±0.005 | 0.087 | ±0.097 |
| 19-ER/ASK-02 | | | | | | | | | | | | | | | |

[a] Major gases and He—Ne isotopes from Byrne et al. (2021).
[b] Measured air-normalized $^3He/^4He$ ratio.
[c] Air-corrected $^3He/^4He$ ratio.
[d] Measured air-normalized $^4He/^{20}Ne$ ratio (Hilton, 1996).

### 5.1. Hydrothermal source fluid composition and secondary processes

The elemental and isotopic compositions of thermal fluids sampled at the surface are affected by shallow secondary processes such as depressurization boiling, mixing, conductive cooling, oxidation and fluid-rock reactions (e.g., Arnórsson et al., 2007). These processes need to be accounted for and quantified in order to estimate the composition of the hydrothermal source fluid, here termed the 'reservoir fluid'.

The temperature and composition of the reservoir fluid of Kverkfjöll, taken to be a single-phase liquid, were reconstructed from the measured compositions of fumaroles and the Hveragil thermal water using the silica-enthalpy method (Fig. S1; Truesdell and Fournier, 1977) and gas thermometers (Arnórsson and Gunnlaugsson, 1985; Arnórsson et al., 1998; Byrne et al., 2021), as well as additional standard techniques outlined in the footnotes of Table 3 and in the Supplementary Information. The silica-enthalpy mixing model yields a reservoir liquid temperature of ~280 °C for Kverkfjöll, which agrees well with major gas thermometers (average of 290±30 °C, 1σ, for $H_2$, $H_2S$, $H_2S$/Ar and $H_2$/Ar thermometers of Arnórsson et al., 1998) and noble gas thermometers (300±30 °C; Byrne et al., 2021). The reconstructed reservoir fluid composition of Kverkfjöll for selected elements is B = 0.8 ppm, Cl = 160 ppm, $SiO_2$ = 530 ppm, $\Sigma CO_2$ = 5400 ppm and ΣS = 200 ppm (Table 3). The full reservoir fluid composition of the Askja system could not be reconstructed, because all thermal spring samples from Askja are affected by condensed fumarole steam (resulting in low pH and high $SO_4$) and no surface outflows of pure or meteoric water-diluted reservoir liquid was found.

**Table 3**
Reservoir fluid compositions.

| Entity | Unit | Kverkfjöll | Askja | Method |
|---|---|---|---|---|
| T | °C | 280±30 | 270±20 | a |
| pH | | 6.8 | | b |
| $SiO_2$ | ppm | 525 | | a |
| B | ppm | 0.76 | | c |
| Na | ppm | 270 | | d |
| K | ppm | 24 | | d |
| Ca | ppm | 0.16 | | d |
| Mg | ppm | 0.002 | | d |
| Fe | ppm | 0.26 | | d |
| Al | ppm | 0.53 | | d |
| F | ppm | 3.71 | | c |
| Cl | ppm | 164 | | c |
| $CO_2$ | ppm | 5400 | 22,100 | e |
| $H_2S$ | ppm | 200 | 450 | e |
| $H_2$ | ppm | 12 | 17 | e |
| $\delta^2H$-$H_2O$ | ‰ | −95.2±4.7 | | f |
| $\delta^{18}O$-$H_2O$ | ‰ | −9.2±1.1 | | f |
| $\delta^{13}C$-$CO_2$ | ‰ | −2.1±1.1 | −3.4±0.4 | g |
| $\delta^{34}S$-$H_2S$ | ‰ | +0.9±1.4 | −0.3±1.3 | h |
| $\Delta^{33}S$-$H_2S$ | ‰ | −0.006±0.010 | −0.012±0.008 | h |

a.
Calculated based on the $SiO_2$-enthalpy geothermometry assuming quartz solubility in the reservoir and adiabatic boiling to 100 °C together with gas $H_2S$/Ar and $H_2$/Ar geothermometry (Arnórsson et al., 1998).
b.
Stefánsson and Arnórsson (2002)
c.
Calculated based on Cl concentration and linear relationship between elemental, $SiO_2$ and Cl aqeuous concentrations.
d.
Based on temperature dependence of ion to proton ratios proposed by Arnórsson et al. (1983) and Stefánsson and Arnórsson (2000)
based on quartz solubility (Gunnarsson and Arnórsson, 2000), adiabatic boiling to 100 °C and $SiO_2$-enthalpy plot.
e.
Based on fumarole vapor compostion and assuming adiabatic boiling to reservoir temperatures and liquid only reservoir fluids.
f.
Calculated from fumarole fluid isotope compostion taking into account adiabatic boiling from reservor liquid to 100 °C and using isotope equilibrium fractionation of Horita and Wesolowski (1994)
g.
Calculated from fumarole fluid isotope composition, taking into account adiabatic boiling from reservor liquid to 100 °C, aqueous and gaseous speciation and assuming isotope equilibrium fractionation. Fractionation factors taken from Stefánsson et al. (2016b). For Askja, the given $\delta^{13}C$ is based on an average and 1σ of $\delta^{13}C$-$CO_2$ values reported by Poreda et al. (1992) and Barry et al. (2014).
h.
Calculated from fumarole fluid isotope composition, taking into account adiabatic boiling from reservor liquid to 100 °C, aqueous and gaseous speciation and assuming isotope equilibrium fractionation. Fractionation factors from Stefánsson et al. (2015)

The δD-$\delta^{18}O$-$\delta^{13}C$-$\Delta^{33}S$-$\delta^{34}S$ signature of the reservoir fluid was estimated from the measured fumarole isotope values by modelling equilibrium isotope fractionation between aqueous and gaseous species upon adiabatic boiling from 280 °C to 100 °C (Fig. 3). The effect of boiling on the speciation of C and S was calculated with the Watch 2.4 software (Bjarnason, 2010). Isotope equilibrium fractionation factors were taken from Horita and Wesolowski (1994) for δD and $\delta^{18}O$, from the compilation of Stefánsson et al. (2016b) for $\delta^{13}C$ and from Stefánsson et al. (2015) for $\Delta^{33}S$ and $\delta^{34}S$. The model details are described in Stefánsson et al. (2015, 2016a, 2017) and in the Supplementary Information.

The δD-$H_2O$ and $\delta^{18}O$-$H_2O$ composition of the reservoir fluid for Kverkfjöll is estimated at −95.2±4.7 ‰ and −9.2±1.1 ‰, which plots on the positive $\delta^{18}O$ side of the GMWL (i.e., has a positive $\Delta^{18}O$ shift). This suggests that the Kverkfjöll reservoir is sourced from a local meteoric groundwater reservoir that experienced considerable water-rock interaction (Fig. 3a). The modelled $\delta^{13}C$-$CO_2$ value of the reservoir fluid is −2.1±1.1 ‰ (Fig. 3d), whereas the $\Delta^{33}S$ and $\delta^{34}S$ ranges of the reservoir fluids are estimated at −0.006±0.010 ‰ (Fig. 3c) and +0.9 ±1.4 ‰, respectively.

Notably, relative to the Kverkfjöll reservoir liquid at depth (280 °C), $H_2O$ vapor at the surface (100 °C) should have more negative δD and $\delta^{18}O$ values, by 16 ‰ and 3.2 ‰, respectively, assuming equilibrium vapor-liquid fractionation during adiabatic boiling (light brown model curve in Fig. 3a).

Thus, depressurization boiling may explain the lower δD-$H_2O$(v) and $\delta^{18}O$-$H_2O$(v) values of most of the fumaroles relative to the reservoir liquid (Fig. 3a). By contrast, the effects of boiling on $\delta^{13}C$-$CO_2$(v) and $\delta^{34}S$-$H_2S$(v) are relatively minor (smaller than −0.5‰ and +1.3 ‰, respectively) (Fig. 3) and the effect on $\Delta^{33}S$-$H_2S$(v) is insignificant (<0.006 ‰) (Supplementary Table 2). Thus, the measured $\delta^{13}C$-$CO_2$(v) and $\delta^{34}S$-$H_2S$(v) values of fumaroles closely reflect the reservoir fluid composition, although the $\delta^{34}S$-$H_2S$(v) values and $H_2S$ concentrations in low-gas flux fumaroles may be affected by additional shallow secondary processes (Fig. S2b). For this reason, only the high-flux fumaroles (defined as those with $CO_2$ > 10 mmol/mol) are considered when evaluating the magmatic source signatures.

### 5.2. Deep magmatic volatile input to volcanic hydrothermal fluids

Magmatic intrusions at ~2–6 km depth below an active volcano may result in the development of an overlying hydrothermal system that transports heat via a circulating fluid from depth to the surface. In addition to heat, intrusions may supply magmatic volatiles to the hydrothermal system via both depressurization degassing, here termed '1st degassing', as well as crystallization-driven degassing, here termed '2nd degassing' (Edmonds and Woods, 2018; Fig. 4a).

To estimate the volatile contribution of 1st degassing to hydrothermal systems, we model the composition of the magmatic gas formed via depressurization degassing from a volatile-undersaturated batch of deep melt to higher crustal levels (Fig. 4; Table S3). As a starting composition, we assume parental melt volatile concentrations of 1 wt% $H_2O$, 4000 ppm $CO_2$, 1400 ppm S and 350 ppm Cl, estimated for Kverkfjöll basalts (Ranta, 2022; Supplementary Information). Using the MagmaSat model

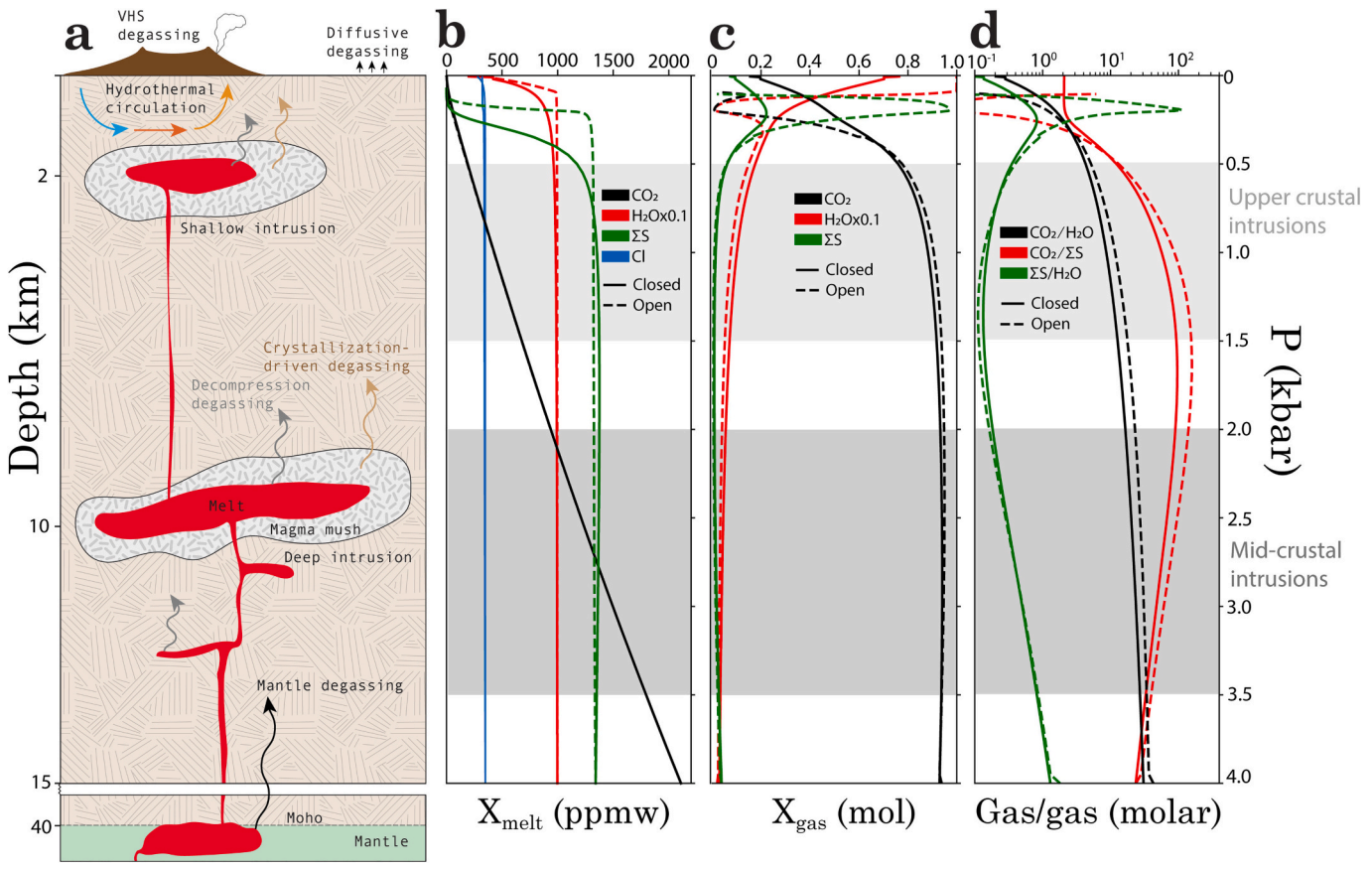


**Fig. 4.** Deep and shallow melt degassing models. (a) Cartoon representing a semi-multi-tiered magmatic system. Ascending melts exsolve magmatic gases via decompression degassing. Further degassing from stalled intrusions occurs via secondary, crystallization-driven degassing, as crystallization of dry minerals keeps residual melts volatile-saturated. The model curves show the composition of (b) melt and (c) magmatic gas during open and closed system degassing between pressures of 4 kbar to 1 bar. (d) The volatile ratios in the magmatic gas change depending on the intrusive pressures. Model curves for $CO_2$, $H_2O$, S and Cl were calculated using SolEx v1.0 (Witham et al., 2012). The Kverkfjöll sample KVK-169 (Ranta et al., 2022) major element composition was used for model calculation along with estimated undegassed volatile concentrations (Supplementary Information).

(Ghiorso and Gualda, 2015) implemented in the VesiCal v1.01 software (Iacovino et al., 2021), a $CO_2$-$H_2O$ saturation pressure of ~5 kbars (~18 km crustal depth) is computed for our model melt. Therefore, pressure below the thick crust of Central Iceland (~30–40 km; Jenkins et al., 2018) is likely to be sufficiently high to suppress direct degassing of mantle-level melts below Askja and Kverkfjöll. For pressures below 4 kbar, we use the SolEx 1.0 program (Witham et al., 2012), which calculates the equilibrium $H_2O$-$CO_2$-S-Cl composition of coexisting melt and gas for open and closed system behavior.

The most important parameters controlling the magmatic gas composition are the initial volatile concentrations of the melt and pressure, i.e., the intrusive depth. We choose 2.5 bars (c. 10 km depth) as a typical Icelandic mid-crustal basaltic magma storage region based on similar depths indicated by geobarometry (Neave and Putirka, 2017; Halldórsson et al., 2018; Caracciolo et al., 2020; Ranta, 2022) as well as seismic and geodetic studies (e.g. Gudmundsson et al., 2016; White et al., 2019). Upon ascent to 2.5 kbar, approximately 70% of the primary $CO_2$ of our model melt is degassed (Fig. 4c) whereas only minor degassing of about 0.3–0.6% $H_2O$, 2–5% S and 0.1–2% Cl is predicted. Further magma ascent to 0.5 kbars, or ~ 2 km, chosen as an approximate upper limit of intrusions (based on the depth of 2100 m where the IDDP-1 drilling at the Krafla volcano in the NRZ encountered a rhyolitic magma body; Mortensen et al., 2014), results in degassing of 95% $CO_2$, 0.6–4% $H_2O$, 6–16% S and 0.2–3% Cl of the initial volatile content of the melt (Fig. 4b).

Characteristically, intrusive magmatic gases formed by decompression degassing have high molar ratios of $CO_2/H_2O$ (~4–40) and $CO_2/\Sigma S$ (~12–160) (Fig. 4d) contrasting with low $CO_2/H_2O$ (<1) and $CO_2/\Sigma S$ (<2) associated with eruptive degassing (cf. Aiuppa et al., 2007). These differences between intrusive and eruptive magmatic gas compositions reflect the higher melt solubilities of $H_2O$ and S relative to $CO_2$ at lower pressures (>0.5 kbar).

Degassing causes isotopic fractionation between the melt and the exsolving gas (Fig. 5). Thus, the magmatic gas will in general have a slightly different $\delta^{13}C$-$\delta^{34}S$ composition from its source melt. We estimate the $\delta^{13}C$-$CO_2$ and $\delta^{34}S$-$\Sigma S$ (where $\Sigma S = H_2S + SO_2$) compositions of magmatic gases degassing from intrusions at different crustal depths by combining elemental degassing model with an isotope fractionation model simulating open and closed system degassing (Fig. 5). For $\delta^{13}C$, we use a source $\delta^{13}C$ signature of −5 ‰, similar to the depleted MORB mantle (DMM) (Marty and Zimmermann, 1999; Barry et al., 2014). Initially, deep magmatic gas has a more positive $\delta^{13}C$-$CO_2$ (as high as −0.2 ‰) relative to the source melt due to a positive vapor-melt fractionation factor ($\Delta^{13}C_{v\text{-}m} = +4.3\pm0.5$ ‰; Barry et al., 2014; see also Javoy et al., 1978). During progressive ascent and closed system degassing, the $\delta^{13}C$-$CO_2$ value of the gas phase approaches the initial melt value, reaching −4.2 ‰ at 2.5 kbar and −4.8 ‰ at 0.5 kbar. On the other hand, extensive open system degassing of $CO_2$ may lead to highly negative gas $\delta^{13}C$-$CO_2$ values (<−10 ‰; Fig. S4). Such low $\delta^{13}C$ values are observed in Icelandic subglacial glasses that are highly degassed with respect to $CO_2$ (Barry et al., 2014), but are not observed in fumarolic $CO_2$. The $\delta^{34}S$-$\Sigma S$(v) becomes either more negative or slightly more positive than initial melt depending on the melt and gas redox states (Mandeville et al., 2009). However, because only minor degassing of S

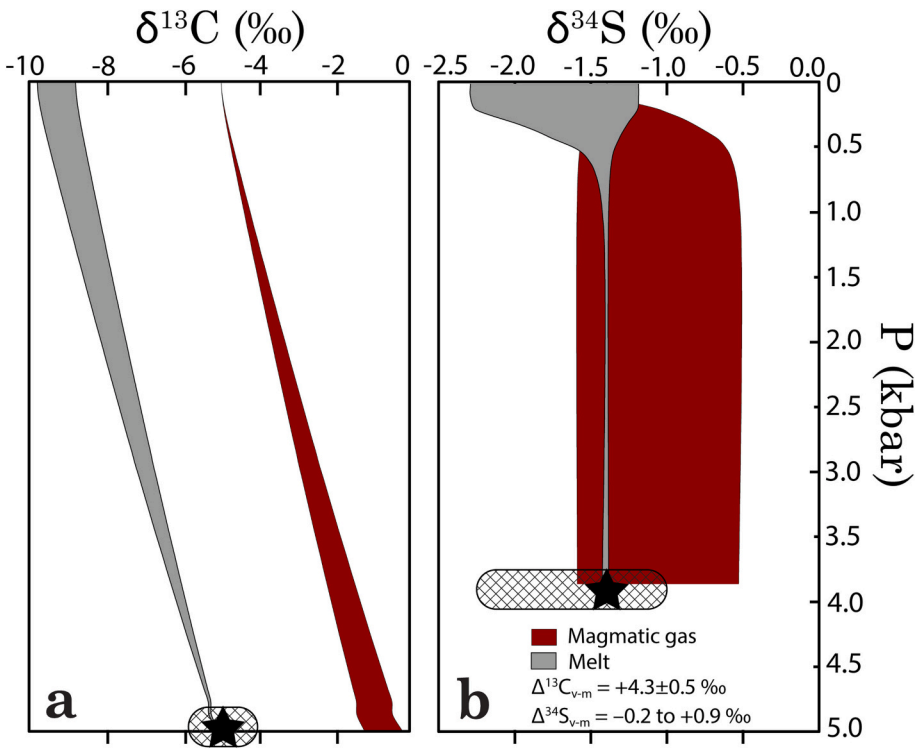


**Fig. 5.** Modelled carbon and sulfur isotopic compositions of magmatic gas upon decompression degassing. (a) $\delta^{13}C$ and (c) $\delta^{34}S$ vs pressure. The isotopic compositions of an exsolved magmatic gas and the residual melt are shown for closed system degassing paths. The $\delta^{13}C$-$CO_2$ value of magmatic gas is initially close to 0 ‰, but becomes lower with decreasing intrusion depth, approaching the initial melt value of −5 ‰. The magmatic gas $\delta^{34}S$-ΣS value may be either slightly more positive or negative depending on the melt and gas redox states (Mandeville et al., 2009). However, because only minor degassing of $H_2O$ and S occur during melt ascent to up to 0.5 kbar, all intrusions have similar $\delta^{34}S$-ΣS values. For $\delta^{13}C$, signature of the depleted MORB mantle (DMM) of −5 ±1 ‰ (Marty and Zimmermann, 1999) is used as the initial melt value, as the $\delta^{13}C$ of the Icelandic mantle is indistinguishable from DMM (Barry et al., 2014). For $CO_2$ degassing, $\Delta^{13}C_{v\text{-}m}$ was chosen as +4.3±0.5 ‰ (Barry et al., 2014). The initial melting composition for $\delta^{34}S$ (−1.39 ‰) is the average Kverkfjöll glass values reported by Ranta et al. (2022). A range of −0.2 to +0.9 ‰ was calculated for the vapor-melt fractionation factor $\Delta^{34}S_{v\text{-}m}$, assuming ranges of $[SO_2/(SO_2 + H_2S)]_v$ = 0.25–0.75 and $[S^{6+}/\Sigma S]_m$ = 0.1–0.2 (see Mandeville et al., 2009 and Ranta et al., 2022 for calculation details).

occurs during melt ascent (~6–16 ‰ up to 0.5 kbar), the $\delta^{34}S$-ΣS values of both deep and shallow magmatic gases remain close to the initial melt signatures (between −1.6 to −0.5 ‰; Fig. 5). Thus, $\delta^{13}C$-$CO_2$ of magmatic gas is a more sensitive indicator of intrusion depth than $\delta^{34}S$ and could potentially be used as a tool to discriminate between deep and shallow magma sources.

Although 2nd degassing of ageing intrusions likely plays an important role in the overall magmatic fluid input into hydrothermal systems, the temporal and compositional evolution of such fluids is a subject of considerable complexity (e.g., Parmigiani et al., 2017) and a detailed volatile degassing model is outside the scope of the present work. Based on the relative solubilities of the main volatiles, a cooling basaltic intrusion should produce a magmatic gas with progressively lower $CO_2$/$H_2O$ and $CO_2$/ΣS, eventually losing all of its initial $CO_2$ and most of its S and $H_2O$. Crystallization of water-poor minerals maintains a cooling intrusion at fluid saturation, leading to a passive supply of magmatic fluids to the hydrothermal domain. Crystallization-driven degassing of intrusions may follow open system degassing paths, producing magmatic gases with much more negative $\delta^{13}C$-$CO_2$ values relative to closed-system degassing (Fig. S4). The $\delta^{34}S$-ΣS signature of magmatic gases produced by 2nd degassing is harder to predict, as both the magnitude and sign of the vapor-melt fractionation factor $\Delta^{34}S_{v\text{-}m}$ will depend on the redox evolution of the intrusion during crystallization (Mandeville et al., 2009; Fig. 5). A factor that complicates the interpretation of VHS volatile signatures is that a single hydrothermal area may simultaneously receive input of magmatic gases from intrusions at different depths and of different ages. Thus, the observed gases at the surface may reflect juxtaposing chemical signals derived from both decompression and crystallization-driven degassing.

Further, we note that the small fraction of magmatic water in meteoric water-dominated VHSs, such as Askja and Kverkfjöll, prevents its detection based on δD-$\delta^{18}O$ values. Assuming that $CO_2$ in fumaroles is derived from magmatic gas ($CO_2/H_2O \approx$ 6–10; Fig. 4d), the proportion of magmatic water in the Askja and Kverkfjöll fumaroles ($CO_2/H_2O$ = 0.002–0.03) is at most 0.3 mol%. This would result in δD and $\delta^{18}O$ shifts of <0.4 ‰ and 0.1‰—similar to the uncertainty of the δD-$\delta^{18}O$ measurements—when assuming δD and $\delta^{18}O$ values for the magmatic water of −50 ‰ and + 4‰, respectively, representative for Kverkfjöll (Marshall et al., 2022; Ranta, 2022). For this reason, trends toward magmatic water components seen in δD-$\delta^{18}O$ graphs at many subduction zone volcanoes (e.g., Giggenbach, 1992; Taran et al., 2018), indicative of degassing of shallow, water-rich magma bodies, have not been observed at Icelandic VHSs.

### 5.3. *Volatile sources and secondary processes*

The $\delta^{13}C$-$CO_2$ and $CO_2$/ΣS values of fumarolic gases can be used to evaluate whether the source of carbon is magmatic gas or leaching (or dissolution) of crustal rocks (Fig. 6). This is possible because the Icelandic crust is igneous, with low $CO_2$/ΣS (~0.003–0.008) and highly negative $\delta^{13}C$-$CO_2$ (<−5 ‰; Barry et al., 2014), contrasting with intrusive magmatic gases that have high $CO_2$/ΣS (>>1) and less negative $\delta^{13}C$-$CO_2$ (>−5 ‰) (Figs. 3d and 6).

The high-flux fumaroles at both Askja and Kverkfjöll converge toward $CO_2$/ΣS of ~13–25 (Figs. S2d and 6a), which we interpret as a primary $CO_2$/ΣS range prior to shallow modifications by secondary processes occurring within the hydrothermal system upon fluid ascent to surface. This range of $CO_2$/ΣS is compatible with magmatic gas originating via decompression degassing from basaltic intrusions at >0.5 kbar (Fig. 6a). Shallower processes in fumarole conduits may influence the $CO_2$/ΣS ratio in low-flux fumaroles. For example, abnormally high $CO_2$/ΣS seen in some low-gas flux Kverkfjöll fumaroles from Efri Hveradalur may result from sulfide fixation (Fig. S2b). $CO_2$ sequestration by hydrothermal calcite in high-temperature hydrothermal systems in Iceland is likely insignificant, based on mantle-like $CO_2/^3He$ and $\delta^{13}C$-$CO_2$ of fumaroles (Barry et al., 2014), and should thus not affect measured $CO_2$/ΣS or $\delta^{13}C$-$CO_2$.

The average fumarolic $\delta^{13}C$-$CO_2$ in Askja is −3.4±0.4 ‰, close to the average of Icelandic VHSs of approximately −4 ‰ (Poreda et al., 1992; Barry et al., 2014). The $\delta^{13}C$-$CO_2$ values of the Kverkfjöll fumaroles (from −4.1 to −0.2‰ with an average of −2.2±1.1 ‰) and the estimated reservoir fluid (−2.1±1.1 ‰) are slightly higher, which could

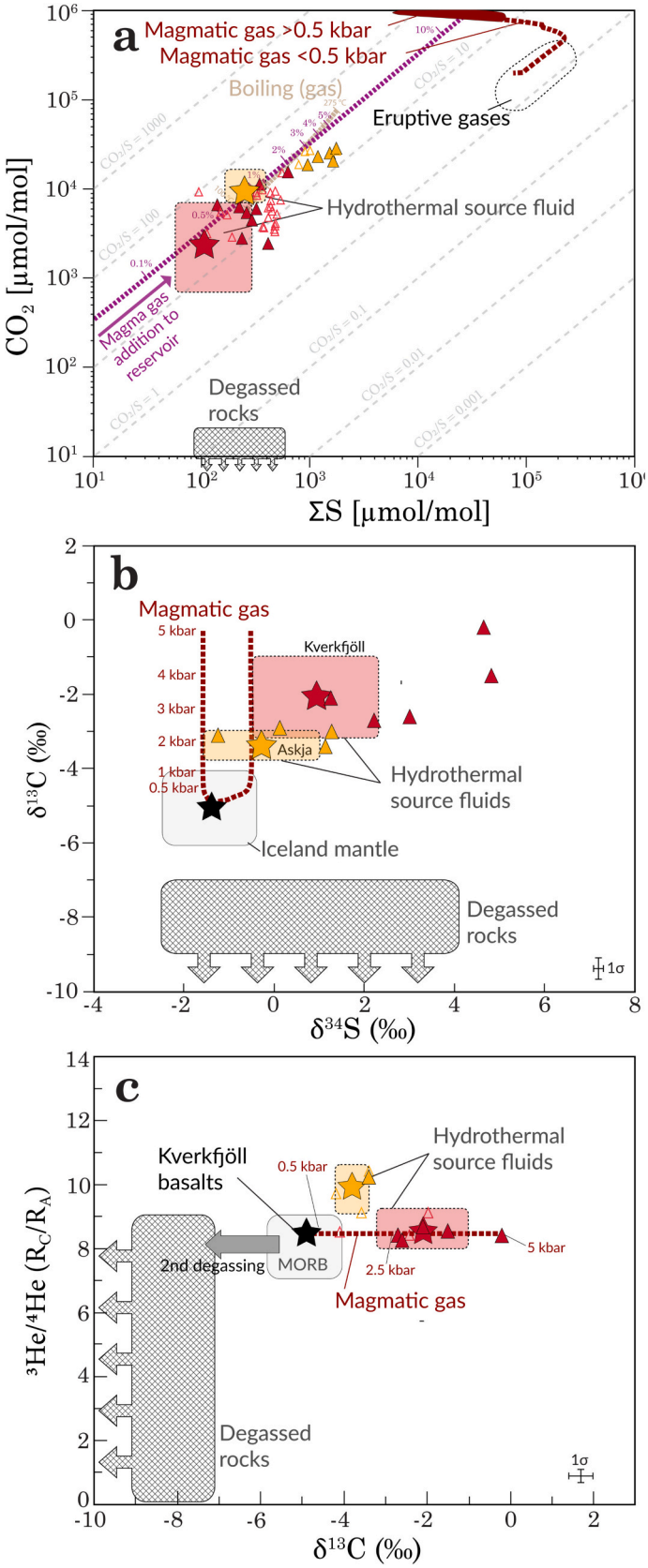


**Fig. 6.** Geochemical signatures of magmatic gases. (a) $CO_2$ versus ΣS. Measured fumarole and estimated reservoir compositions of Kverkfjöll and Askja (red and green stars, respectively) both display $CO_2$/ΣS values that resemble deep (>0.5 kbar) magmatic gases. A mixing line between a meteoric water component and magmatic gas (purple dashed line) implies ~0.5 to 3‰ input of magmatic gas to the reservoir fluid. The effect of depressurization boiling (light brown dashed line) on the $CO_2$/ΣS ratio is small. (b) $\delta^{13}C$ versus $\delta^{34}S$. A field of magmatic gas compositions from closed-system degassing is shown in grey. Subfields show the estimated $\delta^{13}C$ of magmatic gases at a given intrusion pressure. The fields of degassed rocks (brown) are drawn after Torssander (1989), Füri et al. (2010) and Barry et al. (2014). (c) Measured $^3He/^4He$ versus $\delta^{13}C$-$CO_2$. The $\delta^{13}C$-$CO_2$ values of both Askja and Kverkfjöll fumaroles are distributed between the estimated Iceland mantle value (taken as the MORB value of −5±1 ‰; Marty and Zimmermann, 1999; Barry et al., 2014) and more positive $\delta^{13}C$-$CO_2$ values estimated for magmatic gases from intrusions between 0.5 and 5 kbar (crimson dashed line), whereas the $^3He/^4He$ is not affected by degassing and is relatively invariable within each system. This observation is consistent with fumarole $CO_2$ being sourced from decompression degassing of intrusions at different crustal levels, rather than being derived from 2nd degassing or the host rocks, which are likely to have more negative $\delta^{13}C$ relative to source value. (For interpretation of the references to colour in this figure legend, the reader is referred to the web version of this article.)

indicate that $CO_2$ in Kverkfjöll is sourced from deeper (>4 kbar) intrusions (Fig. 6b). Thus, both $CO_2/\Sigma S$ and $\delta^{13}C\text{-}CO_2$ fumarole data suggest that the source of $CO_2$ (and S) at Askja and Kverkfjöll—and at Icelandic VHSs in general—is deep magmatic degassing from basaltic intrusions at various crustal levels from ~2 to ~20 km.

The high concentrations of magmatic $CO_2$ and $H_2S$ in Askja fumaroles relative to other Icelandic hydrothermal systems are consistent with persistent lower crustal intrusive magmatism beneath the central volcano. Seismic tomographic imaging indicates a semi-continuous series of magma storage zones beneath the volcano, with main melt reservoirs located at depths of 5 and 9 km (Mitchell et al., 2013; Greenfield et al., 2016). Deep (~20 km) and frequently occurring earthquake swarms beneath the Öskjuvatn caldera that coincide with a region of slow S-wave velocities indicate a continuous supply of deep magmatic injections to the lower crust (Greenfield and White, 2015; Greenfield et al., 2016). The deep earthquakes, which occur below the brittle-ductile boundary, could be caused by injection of a $CO_2$-rich volatile phase into faults (Greenfield and White, 2015). Decompression degassing of high-frequency deep-sourced melt injections in a multi-tier magma storage system could thus be a feasible source of a near-continuous deep supply of $CO_2$-dominated magmatic gas to the hydrothermal system of Askja and Icelandic volcanoes in general (Greenfield and White, 2015; White et al., 2019).

Like with carbon, sulfur isotope ratios of hydrothermal fluids can help constrain the sources of S, and to identify secondary shallow processes that take place during the upflow (Ohmoto and Lasaga, 1982; Ono et al., 2007; Marini et al., 2011; Stefánsson et al., 2015; Gunnarsson-Robin et al., 2017; Kleine et al., 2021). The reaction pathway of sulfur during its passage from the magma to the surface through a hydrothermal system is more complex than that of carbon due to its multiple redox states ($S^{2-}$, $S^0$, $S^{4+}$, $S^{6+}$). Due to this complexity, the exact reaction pathways remain uncertain, although attempts have been made to account for isotopic fractionation associated with redox reactions, disproportionation, boiling and water-rock reactions (Marini et al., 2011; Stefánsson et al., 2015; Gunnarsson-Robin et al., 2017; Kleine et al., 2021). Dissolution of magmatic gas into an aqueous hydrothermal reservoir likely takes place through disproportionation of magmatic $SO_2(g)$ to $H_2SO_4$ and $H_2S$, but the net effect on the $\delta^{34}S\text{-}\Sigma S$ value of the reservoir fluid is likely to be small relative to shallow hydrothermal processes (Kleine et al., 2021); for example, the fumarole $\delta^{34}S\text{-}H_2S$ can be shifted by up to +1.3 ‰ during decompression boiling upon fluid upflow (Stefánsson et al., 2015). Sequestration of S by pyrite in the hydrothermal reservoir is possible at low water/rock ratios, but would only marginally fractionate the $\delta^{34}S\text{-}H_2S(v)$ value (Marini et al., 2011; Gunnarsson-Robin et al., 2017; Kleine et al., 2021).

The $\delta^{34}S\text{-}H_2S$ values of Askja fumaroles (−1.5 to +1.3 ‰) are similar, or up to 2 ‰ more positive than basaltic, undegassed melts from the NRZ, which have $\delta^{34}S$ values of −2.3 to −0.5 ‰ (Ranta et al., 2022). These values are consistent with derivation of S from deep magmatic gas that experienced a small degree of positive fractionation during adiabatic boiling. The Kverkfjöll fumarole $\delta^{34}S\text{-}H_2S$ values (+1.1 to +4.8 ‰) are considerably more positive than undegassed, basaltic Kverkfjöll melts (−2.3 to −0.9 ‰), which indicates that significant fractionation must have taken place if S in the Kverkfjöll reservoir is sourced directly from magmatic gas. Positive $\delta^{34}S\text{-}H_2S$ could be derived via leaching of degassed silicic host-rocks, which may have positive $\delta^{34}S$ of up to +4.2 ‰ (Torssander, 1989; Ranta et al., 2022). The highest $\delta^{34}S\text{-}H_2S$ value in Kverkfjöll (+4.82 ‰) is found in a fumarole sample that also has the highest oxygen shift ($\Delta^{18}O = +3.87$ ‰), indicating extensive fluid-rock interaction, and low $CO_2$ (2800 μmol/mol), indicating low magmatic gas flux.

Previously measured $\delta^{34}S\text{-}H_2S$ values in Icelandic fumarole vapors span a wider range and are, on average, more positive relative to well discharges from same hydrothermal areas (Gunnarsson-Robin et al., 2017). We interpret these observations to reflect secondary effects imposed by unspecified shallow fumarole conduit processes on the measured $\delta^{34}S\text{-}H_2S$ values. Thus, we consider the $\delta^{34}S\text{-}H_2S$ signatures of fumaroles with higher gas-flux (>10 mmol/mol $CO_2$) to better represent the reservoir fluid signature.

### 5.4. Magmatic volatile fluxes through hydrothermal systems

Several previous studies have attempted to quantify the mantle-to-atmosphere volatile fluxes associated with VHSs (Seward and Kerrick, 1996; McGee et al., 2001; Barry et al., 2014; Stefánsson et al., 2016b; Taran and Kalacheva, 2018). Here, we apply a forward modelling approach, using magmatic gas compositions estimated for intrusions at different crustal levels (Fig. 4). Then, using estimated magma extrusion rates (Thordarson and Larsen, 2007; Thordarson and Höskuldsson, 2008) and assuming intrusive/extrusive magmatism ratios of 4 to 8 (White et al., 2006) we calculate intrusive magmatic degassing potentials for Iceland for $H_2O$, $CO_2$, S and Cl (Table 3; Fig. 7; Supplementary Information). By comparing the magmatic degassing potential to observed volatile fluxes at hydrothermal systems and eruptions, it is possible to put semi-quantitative constraints on the deep volatile fluxes channeled via VHSs versus eruptions. Furthermore, this modelling approach allows us to place qualitative constraints on the relative contributions of decompression and crystallization-driven degassing and crustal leaching to the volatile fluxes in Icelandic VHSs.

We estimate the eruptive $CO_2$ and S fluxes of 120–690 kt/yr and 70–170 kt/yr, respectively, based on estimated erupted basalt volumes from post-glacial (minimum value, 0.04–0.06 $km^3$/yr; Thordardson and Larsen, 2007) and historic (last 1100 years; maximum value; 0.063 $km^3$/yr Thordarson and Höskuldsson, 2008) eruptions (Fig. 7a).

The intrusive flux represents the total amount of volatiles carried by mantle-derived basaltic melts into the crust and atmosphere. This estimate does not differentiate between volatiles released to the atmosphere and volatiles sequestered by the crust. For $CO_2$ and S, the total intrusive flux is equal to the sum of volatiles lost through 1st and 2nd degassing. We estimate an intrusive flux of 470 to 5520 kt/yr for $CO_2$ and 280 to 1380 kt/yr S, based on the eruptive fluxes and an intrusive/extrusive ratio for basaltic magmatism of 4 to 8 (Fig. 7a; Table 4; White et al., 2006).

The 1st degassing potential (magma decompression degassing) is calculated by scaling the intrusive flux by the expected volatile release for two different intrusion pressures, 0.5 and 2.5 kbar (Table S3). For the 2nd degassing potential (magma crystallization-driven degassing) we assume that most of the $CO_2$ and S remaining in magmatic intrusions after decompression degassing is lost via crystallization-driven degassing as the magmas cool and solidify. The validity of this assumption is supported by low concentrations of $CO_2$ (<10 ppm) and S (<200 ppm) in crystalline intrusions relative to undegassed melts (typically >1000 ppm for both $CO_2$ and S; Matthews et al., 2021; Ranta et al., 2022). For $CO_2$ and S, the 2nd degassing flux can thus be estimated by making the approximation.

$$\text{2nd degassing flux} \approx \text{Intrusive flux} - \text{1st degassing flux} \quad (2)$$

A crude estimate of the hydrothermal flux of $CO_2$ and S in Iceland can be made by multiplying the steam flux by a representative fumarole composition, taken here as the average of the Icelandic fumaroles in Byrne et al. (2021). The steam flux can be calculated from estimated hydrothermal power, assuming a heat content of 1.9 kg/s/MW for pure water steam at 100 °C (Stefánsson et al., 2011). Using values between 4000 MW (Björnsson, 2006) and 8000 MW (Bodvarsson, 1982) for the total hydrothermal power of Iceland, we calculate a steam flux of 7600–15,200 kg/s. This yields a hydrothermal flux of 3365–6740 kt/yr $CO_2$ and 220–440 kt/yr S (Table 4). It is worth noting that the higher value seems more compatible with the estimated hydrothermal power of 4550 MW contained in only subglacial geothermal systems beneath Iceland's ice caps (Jóhannesson et al., 2020).

The total volatile fluxes emanating from the Kverkfjöll hydrothermal area was approximated similarly as above but using a hydrothermal heat

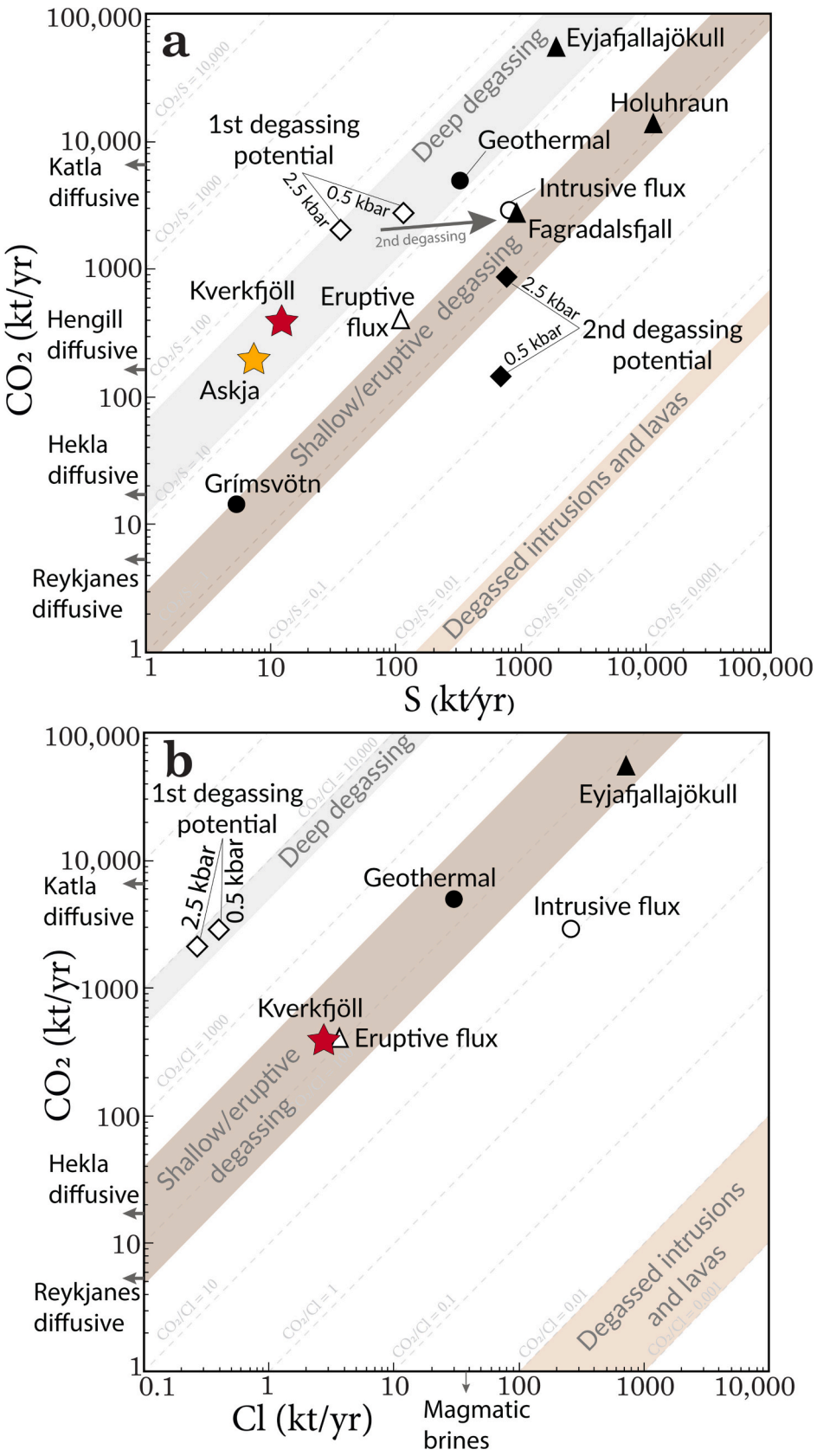


**Fig. 7.** Volatile flux estimates for Icelandic volcanoes and VHSs. (a) Similar $CO_2/\Sigma S$ to between Icelandic VHSs and estimated magmatic gas compositions suggest that intrusive degassing is a plausible supplier of both $CO_2$ and S to VHSs in Iceland. Crustal leaching must play only a minor role in the supply of $CO_2$ and S, because degassed intrusions and lavas that make up the upper Icelandic crust have very low $CO_2/\Sigma S$ (0.003–0.008). (b) By contrast, degassed crustal rocks retain most of their primary Cl content and are likely the main source of Cl in hydrothermal reservoir liquids. For clarity, only calculated mean values are displayed.

**Table 4**
Flux estimates.

| Type | Reference | Method | $CO_2$ (kt/yr) | | | S (kt/yr) | | | $H_2O$ (kt/yr) | | Cl (kt/yr) | | | $CO_2/\Sigma S$ | |
|---|---|---|---|---|---|---|---|---|---|---|---|---|---|---|---|
| | | | min | max | avg | min | max | avg | min | max | avg | min | max | avg | by mass |
| *Iceland total flux* | | | | | | | | | | | | | | | |
| Iceland (total $CO_2$) | Barry et al. (2014) | He flux and $CO_2/^3He$ | 88 | 10,122 | 5105 | | | | | | | | | | |
| Iceland (total $CO_2$) | Stefánsson et al. (2016b) | $\delta^{13}C$, heat output | 2200 | 4401 | 3301 | | | | | | | | | | |
| Iceland (intrusive potential)[b] | Ármansson et al. (2005) | Magmatic flux | | | 1300 | | | | | | | | | | |
| Iceland (intrusive potential) | *This study* | Magmatic flux | 466 | 5328 | 2897 | 280 | 1332 | 806 | 932 | 13,320 | 7126 | 47 | 466 | 256 | 3.6 |
| Iceland eruptive flux[a] | *This study* | Solubility model+magma flux | 117 | 690 | 403 | 63 | 155 | 109 | 163 | 1208 | 685 | 1.2 | 6.0 | 3.6 | 3.7 |
| *Intrusive degassing fluxes* | | | | | | | | | | | | | | | |
| 1st degassing (2.5 kbar) | *This study* | Solubility model+magma flux | 326 | 3730 | 2028 | 5.6 | 67 | 36 | 2.8 | 80 | 41 | 0.0 | 9.3 | 4.7 | 56 |
| 1st degassing (0.5 kbar) | *This study* | Solubility model+magma flux | 443 | 5062 | 2752 | 17 | 213 | 115 | 5.6 | 533 | 269 | 0.1 | 14.0 | 7.0 | 24 |
| 2nd degassing (2.5 kbar) | *This study* | Solubility model+magma flux | 140 | 1598 | 869 | 274 | 1265 | 770 | | | | | | | 1.1 |
| 2nd degassing (0.5 kbar) | *This study* | Solubility model+magma flux | 23 | 266 | 145 | 263 | 1119 | 691 | | | | | | | 0.2 |
| *Icelandic volcanoes* | | | | | | | | | | | | | | | |
| Fagradalsgjall 2021[c] | Halldórsson et al. (2022) | Petrological method | | | 2700 | | | 930 | | | | | | | 2.9 |
| Eyjafjallajökull 2010 | Allard et al. (2011) | Direct measurement | | | 54,788 | 1644 | 2192 | 1918 | | | 262,980 | | | 708 | 29 |
| Holuhraun 2014–15 | Bali et al. (2018) | Petrological method | 11,972 | 15,625 | 13,798 | | | 11,477 | 45,048 | | | | | | 1 |
| *Geothermal degassing* | | | | | | | | | | | | | | | |
| Iceland geothermal[d] | *This study* | Heat output | 3365 | 6730 | 5047 | 220 | 440 | 330 | 236,000 | 472,000 | 354,000 | 0.1 | 41.3 | 20.7 | 15 |
| Grímsvötn | Ágústsdóttir and Brantley (1994) | Caldera lake composition | | | 14 | 5.3 | 23 | 5.3 | | | | | | | 3 |
| Kverkfjöll | *This study* | Heat output | 292 | 497 | 395 | 9.0 | 15 | 12 | 11,688 | 19,870 | 15,779 | | | | 32 |
| Askja geothermal | *This study* | Caldera lake composition | 14 | 389 | 201 | 0.5 | 14 | 7.3 | | | | | | | 27 |
| *Diffusive degassing* | | | | | | | | | | | | | | | |
| Reykjanes, diffusive | Fridriksson et al. (2006) | Direct measurement | 4.4 | 5.7 | 5.1 | | | | | | | | | | |
| Hekla, diffusive | Ilyinskaya et al. (2015) | Direct measurement | | | 16 | | | 0.002 | | | | | | | 10,000 |
| Hengill, diffusive | Hernández et al. (2012) | Direct measurement | 150 | 181 | 165 | | | 0.003 | | | 14,656 | | | | 56,600 |
| Katla, diffusive | Ilyinskaya et al. (2018) | Airborne measurement | 4380 | 8760 | 6570 | | | | | | | | | | >100 |

[a] Assuming degassing of 100% $CO_2$, 90% S, 70% $H_2O$ and 10% Cl, based on decompression degassing to 1 bar.

[b] Based on estimated magmatic flux of $5.8 \times 10^{11}$ kg/yr with melt $CO_2$ concentration of 2200 ppm.

[c] Calculated with the petrological method (Devine et al., 1984) using the difference between maximum melt inclusion (1171 ppm S and 3525 ppm $CO_2$; a single outlier with 5962 ppm $CO_2$ filtered out) and minimum matrix glass contents (0 ppm for both) in Halldórsson et al. (2022), an erupted volume of $150 \times 10^6$ $m^3$ over 180 days (Pedersen et al., 2022) and assuming lava density of 2600 kg/m3 (Bali et al., 2018).

[d] The geothermal $CO_2$ and S fluxes are based on average fumarole concentrations in Byrne et al. (2021). Minimum Cl flux is based on the average Cl concentrations in Krafla fumaroles ($0.44 \pm 0.5$ ppm, $1\sigma$, $n = 12$; Stefánsson and Barnes, 2016) and represents atmospheric emissions of Cl. Maximum Cl flux estimate is based on average Cl concentration in Geysir, Flúðir, Hellisheiði, Krafla, Nesjavellir and Krafla reservoir liquids ($86 \pm 59$ ppm, $1\sigma$, $n = 35$; Stefánsson and Barnes, 2016) and represent the Cl flux of meteoric-water dominated hydrothermal liquids. All values, and the $H_2O$ flux, are scaled to total geothermal power of 4–8 GW (Björnsson, 2006; Bodvarsson, 1982) and assuming 1.9 kg $H_2O$ steam/s/MW (Stefánsson et al., 2011).

output of 270±70 MW (Oddsson, 2016), equivalent to a steam flux of 380–650 kg/s, and the average composition of 11 Hveratagl fumaroles (Ólafsson et al., 2000; Byrne et al., 2021) that have relatively high gas flux and are assumed to be less affected by shallow S or C sequestration. This yields $CO_2$ and S fluxes of 290–500 kt/yr and 9–15 kt/yr, respectively.

Because the heat output of Askja is poorly constrained, we made a crude estimate of the hydrothermal volatile fluxes at Askja by assuming that (1) the high $SO_4$ concentrations (80–880 ppm, average 450 ppm; Ólafsson, 1980; this study) of Lake Öskjuvatn are derived from quantitative condensation and oxidation of fumarolic $H_2S$ that pass through the local aquifer (Fig. 8a), and that (2) the lake has a freshwater recharge of 48 Mt./yr (Ólafsson, 1980). Then, the average S flux is calculated as

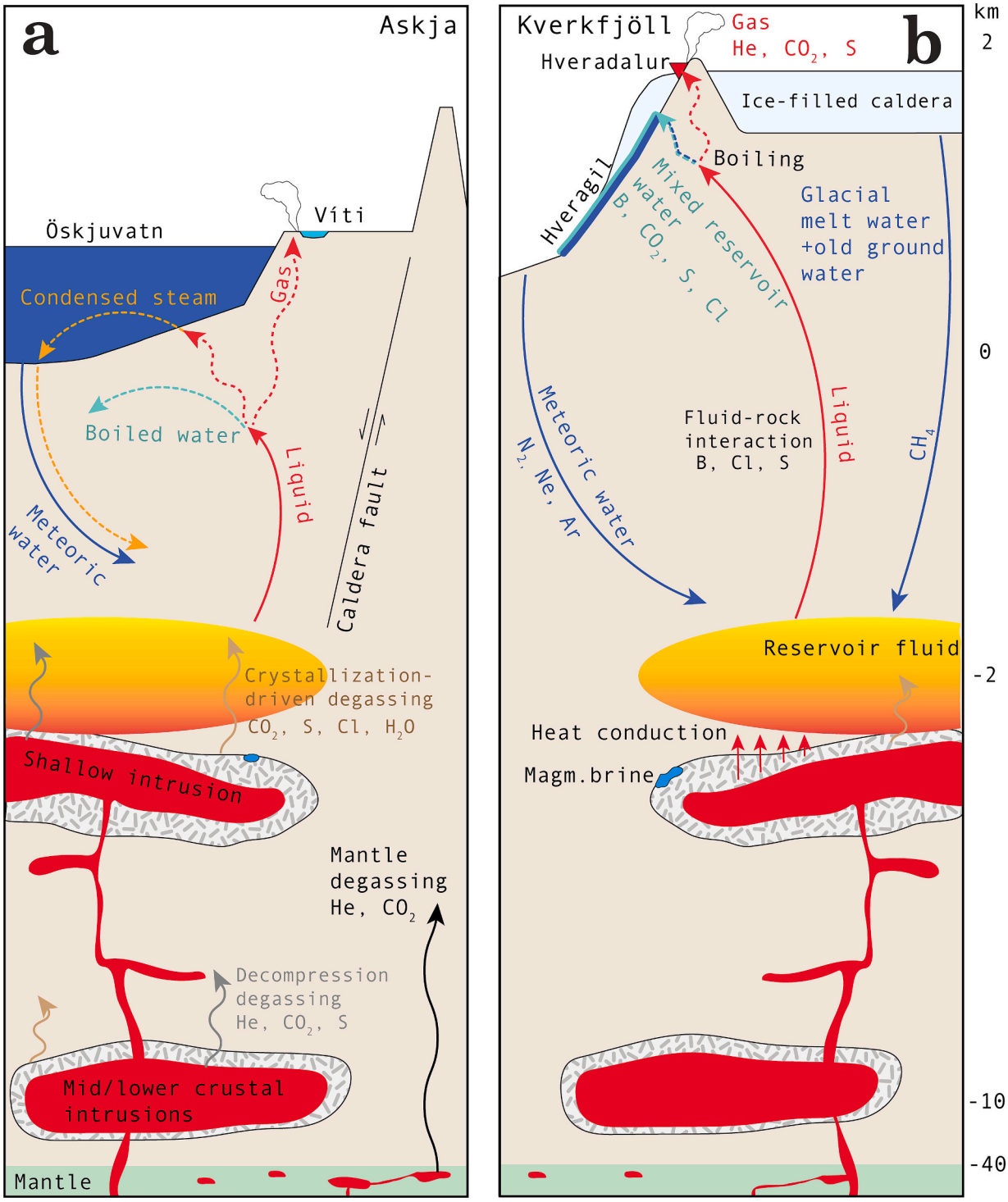


**Fig. 8.** Summary figure illustrating the volatile sources at the volcanic hydrothermal systems of (a) Askja and (b) Kverkfjöll. The differing thermal surface manifestations are largely dictated by the contrasting topography between Askja (flat) and Kverkfjöll (steep), whereas the magmatic roots underlying the hydrothermal reservoirs of the two systems are conceptually similar (see Supplementary Information). Deep decompression degassing is the main source of He, $CO_2$ and S in the hydrothermal fluids. Secondary, crystallization-driven degassing and/or crustal leaching may be secondary sources of S, and provide small amounts of magmatic $H_2O$ and Cl.

Average S flux = Freshwater recharge × average S concentration in lake water (3)

This yields an average fumarolic S flux of 7 kt/yr for Askja. The flux of $CO_2$, which is not quantitatively scrubbed by the shallow aquifer (Ilyinskaya et al., 2015), cannot be estimated in the same way. Instead, if the average $CO_2/H_2S$ of the Víti fumaroles is taken to be representative of the Askja hydrothermal fluids, the $CO_2$ flux can be estimated as 200 kt/yr. These yield a total steam flux of 103 kg/s or ≈ 3 Mt/yr, which correspond to 6.25% of the total inflow of freshwater into Lake Öskjuvatn, or an equivalent heat output of 196 MW.

### 5.5. Mantle to surface fluxes of volatiles ($H_2O$, C, S, Cl)

Previous studies have estimated the total volcanic mantle-to-atmosphere $CO_2$ fluxes in Iceland of 88–10,122 kt/yr (Barry et al., 2014; the lower value is likely to be an underestimate, as it was calculated based on very low melt $CO_2$ concentration and basalt production rate estimates of 531 ppm and 0.064 $km^3$/yr, respectively), 1300 kt/yr (Ármannsson et al., 2005) and 2200–4401 kt/yr (Stefánsson et al., 2016b). These values are higher than our estimate for the eruptive $CO_2$ flux of 120–690 kt/yr, but similar to our estimate of the intrusive $CO_2$ flux (470–5520 kt). The similarity between the $CO_2$ flux estimates suggests that (1) an intrusive:extrusive ratio of 4 to 8 is a reasonable estimate for Iceland, agreeing well with the 4–8:1 ratio estimated by White et al. (2006), and that (2) quiescent volcanic $CO_2$ degassing via VHSs is likely to account for >75% of the total magmatic $CO_2$ flux, whereas $CO_2$ released during eruptions only accounts for a minor part (<25%) of the total flux. Importantly, the independently calculated estimates for hydrothermal and intrusive $CO_2$ fluxes overlap (Fig. 7). This suggests that basaltic intrusions vent a large part of their primary $CO_2$ load through hydrothermal systems (Fig. 8). The relative role between VHS outgassing and diffusive outlets is not well constrained. Existing estimates of diffusive $CO_2$ degassing in active Icelandic volcanoes vary from relatively low for Reykjanes (4–6 kt/yr; Fridriksson et al., 2006) and Hekla (16 kt/yr; Ilyinskaya et al., 2015) to potentially extremely high for Katla (4380–8760 kt/yr; Ilyinskaya et al., 2018). The high estimate for Katla is anomalous, as it is similar to the entire estimated intrusive $CO_2$ flux of Iceland, and half of the $CO_2$ emissions rate of the 2014–15 Holuhraun eruption (12000–15,600 kt/yr; Bali et al., 2018), which lasted for 6 months and was the largest fissure eruption in Iceland in 230 years, erupting 1.44 $km^3$ of basaltic lava (Pedersen et al., 2017).

Indeed, such high $CO_2$ flux, if maintained, would need to be sourced from an enormous inflow of deep-sourced melt corresponding to about 0.5 to 1 $km^3$/yr, assuming degassing of ~3000 ppm $CO_2$/kg melt with a density of 2700 kg/$m^3$. Such high melt production beneath Katla seems unrealistic (e.g., it would be noticed by the extensive GPS and seismic monitoring network at Katla). Thus, taken at face value, the extremely high $CO_2$ flux estimate for Katla could reflect either a transient phenomenon (a gas pulse or inflow of a fresh batch of magma) or a vastly higher $CO_2$ concentration in the Katla melts relative to our estimate. Thus, we do not consider the high suggested $CO_2$ flux for Katla to be representative of typical quiescent $CO_2$ fluxes at active Icelandic volcanoes. Importantly, a comparison between 1st degassing and total intrusive fluxes demonstrates that decompression degassing of basaltic intrusions is sufficient to account for the flux of $CO_2$ to Icelandic VHSs.

Whereas passive $CO_2$ degassing occurs through soils or via low-T groundwaters outside the realm of VHSs in Iceland (Gislason et al., 1992; Fridriksson et al., 2006; Hernandéz et al. 2012, Ilyinskaya et al., 2015; Stefánsson et al., 2016b), sulfur outgassing is typically negligible outside of hydrothermal areas. Thus, the flux of $H_2S$ in fumaroles is a direct measure of quiescent magmatic sulfur fluxes to the atmosphere (McGee et al., 2001). Notably, the hydrothermal S flux estimated here (220–440 kt/yr) is larger than the average atmospheric flux of S from eruptions (60–170 kt/yr). However, it should be noted that of the total hydrothermal S flux, a poorly constrained proportion is sequestered into shallow aquifers by near-surface condensation and oxidation of fumarolic $H_2S$ and does not necessarily enter the atmosphere.

For S, the gap between the magmatic 1st degassing flux (6–210 kt/yr S) and the total intrusive S flux potential (280–1380 kt/yr) is larger than for $CO_2$ (Fig. 7a) because of its higher relative solubility at intrusive pressures. Instead, most of the remaining intrusive S flux is expected to be lost from intrusions during 2nd degassing (estimated at 270–1270 kt/yr). Cooling intrusions in a multi-tiered crustal plumbing system could provide a persistent flux of S to VHSs via 2nd degassing. However, the hydrothermal S flux estimated here is intermediate (220–440 kt/yr) between 1st and 2nd degassing fluxes, possibly hinting that at least some S is naturally sequestered in the crust (Gunnarsson-Robin et al., 2020), as is the case at submarine VHSs at mid-ocean ridges (Kleine et al., 2022). Another possible source of S to VHSs is leaching of host rocks (Gunnarsson-Robin et al., 2017), as the S concentration of basaltic lavas and intrusions is small but not negligible (10–350 ppm, or up to 20% of the S in undegassed basaltic melts; Torssander, 1989). Because the $\Delta^{34}S_{gas\text{-}melt}$ fractionation factor is poorly constrained (i.e., it may be either positive or negative), and due to possible $\delta^{34}S$ fractionation during shallow hydrothermal reactions, the $\delta^{34}S$-$H_2S$ values of the fumarole gases cannot be conclusively used to separate between 2nd degassing and crustal leaching.

Estimating fluxes of Cl and $H_2O$ is more complicated than for $CO_2$ or S because of their higher solubility in basaltic melts, as well as their potential sequestration in late-stage hydrous and chloride minerals and hydrosaline magmatic volatile phases (Webster, 2004; Webster et al., 2015; Kleine et al., 2020; Ranta et al., 2021). We estimate that mantle-derived $H_2O$ and Cl are transported by intrusions to the Icelandic crust at a rate of 930–13,300 kt/yr and 50–470 kt/yr, respectively. However, only a small fraction of $H_2O$ (3–530 kt/yr), and especially of Cl (0.05–14 kt/yr), is lost during 1st degassing due to the high solubility of both volatiles at the chosen upper limit of intrusion pressures (0.5 kbar). Second degassing induced by crystallization of magmas leads to exsolution of hydrosaline fluids or brines during late-stage evolution of silicic melts (Webster, 2004) amounting to approximately 2–32 kt/yr Cl in Iceland (Ranta et al., 2021). Because of their higher density relative to groundwater, brines are not easily incorporated into hydrothermal convection cells and may remain stagnant in the crust (Afanasyev et al., 2018). Instead, the estimated hydrothermal flux of Cl (0.1–41 kt/yr), based on average Cl concentrations of fumaroles (lower estimate) and reservoir liquids (higher estimate) of Stefánsson and Barnes (2016), is presumably mainly due to remobilization of crustal Cl by high-temperature water-rock interaction occurring within the hydrothermal system itself (Stefánsson and Barnes, 2016).

## 6. Conclusions

This study demonstrates that the composition of natural hydrothermal fluids can be used together with chemical, isotope, and volatile solubility modelling to distinguish and quantify the contributions of magmatic volatile fluxes in volcanic hydrothermal systems and their emissions to the surface. The isotope ($\delta^{13}C$-$CO_2$ and $\Delta^{33}S$ and $\delta^{34}S$-$H_2S$) and abundance ($CO_2/\Sigma S$) signatures in fumarole gases are similar to modelled compositions of deep magmatic gases, suggesting that melt degassing from intrusive magmatism is the main source of $CO_2$ and S in Icelandic volcanic hydrothermal systems. Mass balance calculations of estimated mantle $CO_2$ fluxes in Iceland suggest that most $CO_2$ degassed via VHSs (~3360–7720 kt/yr) is likely to be derived from decompression degassing of basaltic magmas as they move from the mantle to the upper crust. However, decompression degassing of melts appears insufficient to supply the observed VHS flux of S, accounting for only 25–100%. Instead, leaching of host rock and crystallization-driven degassing of maturing intrusions below hydrothermal areas are suggested as additional sources of S to VHSs. By contrast, the majority of the mantle flux of Cl (~50–470 kt/yr) is retained in the crust, as its high solubility in basalts leads to only minor intrusive (0–14 kt/yr) and

eruptive (1–6 kt/yr) degassing. Instead, remobilization of crustal Cl by high-T water-rock interaction (0.1–41 kt/yr) and formation of magmatic brine (2–32 kt/yr) are proposed as the main mechanisms that redistribute mantle-derived Cl in the crust.

## Declaration of Competing Interest

The authors declare that they have no known competing financial interests or personal relationships that could have appeared to influence the work reported in this paper.

## Data availability

The supplementary tables include sample information and the full geochemical dataset as well as a summary of modelling results

## Acknowledgements

ER gratefully acknowledges funding from the Nordic Volcanological Center and the University of Iceland Doctoral Research Fund. SAH acknowledges funding from the Icelandic Research Fund (Grant #196139-051). Iceland Glaciological Society, Kate Gallagher, Karl Stefánsson, Maja Bar Rasmussen, Matt Jackson, Ed Marshall, Dan Colman, Margaret Hartley, Guðmundur Guðfinnsson, Dave Byrne, Mike Broadley and Arola Moreras Marti are thanked for their enormous help and grit during occasionally harsh field conditions. Rósa Ólafsdóttir is thanked for ensuring superb water isotope data. Ríkey Kjartansdóttir is thankfully acknowledged for lab support and ICP-OES analyses. Gareth Izon at MIT provided expert help during off-hours when the sulfur line was having hiccups. The authors are thankful for the reviews of Yuri Taran and Tobias Fischer, whose suggestions helped improve the quality of the manuscript.

## Appendix A. Supplementary data

Supplementary data to this article can be found online at https://doi.org/10.1016/j.jvolgeores.2023.107776.

## References

Afanasyev, A., Blundy, J., Melnik, O., Sparks, S., 2018. Formation of magmatic brine lenses via focussed fluid-flow beneath volcanoes. Earth Planet. Sci. Lett. 486, 119–128.
Ágústsdóttir, A.M., Brantley, S.L., 1994. Volatile fluxes integrated over four decades at Grímsvötn volcano, Iceland. J. Geophys. Res. Solid Earth 99 (B5), 9505–9522.
Aiuppa, A., Moretti, R., Federico, C., Giudice, G., Gurrieri, S., Liuzzo, M., Papale, P., Shinohara, H., Valenza, M., 2007. Forecasting Etna eruptions by real-time observation of volcanic gas composition. Geology 35 (12), 1115–1118.
Aiuppa, A., Fischer, T.P., Plank, T., Bani, P., 2019. $CO_2$ flux emissions from the Earth's most actively degassing volcanoes, 2005–2015. Sci. Rep. 9 (1), 1–17.
Allard, P., Burton, M., Oskarsson, N., Michel, A., Polacci, M., 2011. Magmatic gas composition and fluxes during the 2010 Eyjafjallajökull explosive eruption: implications for degassing magma volumes and volatile sources. In: Geophysical Research Abstracts, Vol. 13.
Alt, J.C., Shanks III, W.C., 1998. Sulfur in serpentinized oceanic peridotites: Serpentinization processes and microbial sulfate reduction. J. Geophys. Res. Solid Earth 103 (B5), 9917–9929.
Andres, R.J., Kasgnoc, A.D., 1998. A time-averaged inventory of subaerial volcanic sulfur emissions. J. Geophys. Res.-Atmos. 103 (D19), 25251–25261.
Ármannsson, H., 2016. The fluid geochemistry of Icelandic high temperature geothermal areas. Appl. Geochem. 66, 14–64.
Ármannsson, H., Fridriksson, T., Kristjánsson, B.R., 2005. $CO_2$ emissions from geothermal power plants and natural geothermal activity in Iceland. Geothermics 34 (3), 286–296.
Árnason, B., 1976. Groundwater systems in Iceland traced by deuterium. Publ. Soc. Sci. Isl. 42, 236.
Arnórsson, S., Gunnlaugsson, E., 1985. New gas geothermometers for geothermal exploration—calibration and application. Geochim. Cosmochim. Acta 49 (6), 1307–1325.
Arnórsson, S., Fridriksson, Th., Gunnarsson, I., 1998. Gas chemistry of the Krafla geothermal field, Iceland. In: Arehart, G.B., Hulston, J.R. (Eds.), Water-Rock Interaction 8. Balkema, Rotterdam, pp. 613–616.
Arnórsson, S., Bjarnason, J.Ö., Giroud, N., Gunnarsson, I., Stefánsson, A., 2006. Sampling and analysis of geothermal fluids. Geofluids 6 (3), 203–216.
Arnórsson, S., Stefánsson, A., Bjarnason, J.O., 2007. Fluid-fluid interactions in geothermal systems. Rev. Mineral. Geochem. 65 (1), 259–312.
Bali, E., Hartley, M.E., Halldórsson, S.A., Gudfinnsson, G.H., Jakobsson, S., 2018. Melt inclusion constraints on volatile systematics and degassing history of the 2014–2015 Holuhraun eruption, Iceland. Contrib. Mineral. Petrol. 173 (2), 1–21.
Barry, P.H., Hilton, D.R., Füri, E., Halldórsson, S.A., Grönvold, K., 2014. Carbon isotope and abundance systematics of Icelandic geothermal gases, fluids and subglacial basalts with implications for mantle plume-related CO2 fluxes. Geochim. Cosmochim. Acta 134, 74–99.
Barry, P.H., De Moor, J.M., Chiodi, A., Aguilera, F., Hudak, M.R., Bekaert, D.V., Turner, S.J., Curtice, J., Seltzer, A.M., Jessen, G.L., Osses, E., Blamey, J.M., Amenábar, M.J., Selci, M., Cascone, M., Bastianoni, A., Nakagawa, M., Filipovich, R., Bustos, E., Schrenk, M.O., Buongiorno, J., Ramirez, C.J., Rogers, T.J., Lloyd, K.G., Giovannelli, D., 2022. The helium and carbon isotope characteristics of the Andean convergent margin. Front. Earth Sci. 10, 897267.
Bekaert, D.V., Turner, S.J., Broadley, M.W., Barnes, J.D., Halldórsson, S.A., Labidi, J., Wade, J., Walowskim, K.J., Barry, P.H., 2021. Subduction-driven volatile recycling: A global mass balance. Annu. Rev. Earth Planet. Sci. 49, 37–70.
Bjarnason, J.Ö., 2010. The Speciation Program WATCH Version 2.4, User's Guide. Iceland water chemistry group, Reykjavik, 9 pp.
Björnsson, S., 2006. Geothermal power capacity. Energy Conf. 2006, 332–342 (in Icelandic).
Bodvarsson, G., 1982. Terrestrial energy currents and transfer in Iceland. Cont. Ocean Rifts 8, 271–282.
Byrne, D.J., Broadley, M.W., Halldórsson, S.A., Ranta, E., Ricci, A., Tyne, R.L., Stefánsson, A., Ballentine, C.J., Barry, P.H., 2021. The use of noble gas isotopes to trace subsurface boiling temperatures in Icelandic geothermal systems. Earth Planet. Sci. Lett. 560, 116805.
Caracciolo, A., Bali, E., Guðfinnsson, G.H., Kahl, M., Halldórsson, S.A., Hartley, M.E., Gunnarsson, H., 2020. Temporal evolution of magma and crystal mush storage conditions in the Bárðarbunga-Veiðivötn volcanic system, Iceland. Lithos 352, 105234.
Craig, H., 1963. The isotopic geochemistry of water and carbon in geothermal areas. In: Nuclear Geology on Geothermal Areas. CNR, Pisa, pp. 17–53.
Devine, J.D., Sigurdsson, H., Davis, A.N., Self, S., 1984. Estimates of sulfur and chlorine yield to the atmosphere from volcanic eruptions and potential climatic effects. J. Geophys. Res. Solid Earth 89 (B7), 6309–6325.
Edmonds, M., Woods, A.W., 2018. Exsolved volatiles in magma reservoirs. J. Volcanol. Geotherm. Res. 368, 13–30.
Fiebig, J., Chiodini, G., Caliro, S., Rizzo, A., Spangenberg, J., Hunziker, J.C., 2004. Chemical and isotopic equilibrium between $CO_2$ and $CH_4$ in fumarolic gas discharges: generation of $CH_4$ in arc magmatic-hydrothermal systems. Geochim. Cosmochim. Acta 68 (10), 2321–2334.
Fiebig, J., Woodland, A.B., Spangenberg, J., Oschmann, W., 2007. Natural evidence for rapid abiogenic hydrothermal generation of $CH_4$. Geochim. Cosmochim. Acta 71, 3028–3039.
Fiebig, J., Stefansson, A., Ricci, A., Tassi, F., Viveiros, F., Silva, S., Lopez, T.M., Schreiber, C., Hofmann, S., Mountain, B.W., 2019. Abiogenesis not required to explain the origin of volcanic-hydrothermal hydrocarbons. Geochem. Perspect. Letters 11, 23–27.
Fischer, T.P., 2008. Fluxes of volatiles ($H_2O$, $CO_2$, $N_2$, Cl, F) from arc volcanoes. Geochem. J. 42 (1), 21–38.
Fischer, T.P., Aiuppa, A., 2020. AGU Centennial Grand Challenge: Volcanoes and deep carbon global CO2 emissions from subaerial volcanism—recent progress and future challenges. Geochem. Geophys. Geosyst. 21 (3) e2019GC008690.
Fridriksson, T., Kristjánsson, B.R., Armannsson, H., Margrétardóttir, E., Ólafsdóttir, S., Chiodini, G., 2006. $CO_2$ emissions and heat flow through soil, fumaroles, and steam heated mud pools at the Reykjanes geothermal area, SW Iceland. Appl. Geochem. 21 (9), 1551–1569.
Füri, E., Hilton, D.R., Halldórsson, S.A., Barry, P.H., Hahm, D., Fischer, T.P., Grönvold, K., 2010. Apparent decoupling of the he and Ne isotope systematics of the Icelandic mantle: the role of he depletion, melt mixing, degassing fractionation and air interaction. Geochim. Cosmochim. Acta 74 (11), 3307–3332.
Gerlach, T.M., 1989. Degassing of carbon dioxide from basaltic magma at spreading centers: II. Mid-oceanic ridge basalts. J. Volcanol. Geotherm. Res. 39 (2–3), 221–232.
Gerlach, T.M., 1991. Present-day $CO_2$ emissions from volcanos. EOS Trans. Am. Geophys. Union 72 (23), 249–255.
Ghiorso, M.S., Gualda, G.A.R., 2015. An $H_2O$–$CO_2$ mixed fluid saturation model compatible with rhyolite-MELTS. Contrib. Mineral. Petrol. 169, 1–30.
Giggenbach, W.F., 1992. Isotopic shifts in waters from geothermal and volcanic systems along convergent plate boundaries and their origin. Earth Planet. Sci. Lett. 113 (4), 495–510.
Graham, D.W., 2002. Noble gas isotope geochemistry of mid-ocean ridge and ocean island basalts: Characterization of mantle source reservoirs. Rev. Mineral. Geochem. 47 (1), 247–317.
Greenfield, T., White, R.S., 2015. Building Icelandic igneous crust by repeated melt injections. J. Geophys. Res. Solid Earth 120 (11), 7771–7788.
Greenfield, T., White, R.S., Roecker, S., 2016. The magmatic plumbing system of the Askja central volcano, Iceland, as imaged by seismic tomography. J. Geophys. Res. Solid Earth 121 (10), 7211–7229.
Gudmundsson, M.T., Jónsdóttir, K., Hooper, A., Holohan, E.P., Halldórsson, S.A., Ófeigsson, B.G., Aiuppa, A., 2016. Gradual caldera collapse at Bárdarbunga volcano, Iceland, regulated by lateral magma outflow. Science 353 (6296), aaf8988.
Gunnarsson-Robin, J., Stefánsson, A., Ono, S., Torssander, P., 2017. Sulfur isotopes in Icelandic thermal fluids. J. Volcanol. Geotherm. Res. 346, 161–179.

Gunnarsson-Robin, J., Stefansson, A., Ono, S., Gunnarsson, I., Aradottir, E.S., 2020. $H_2S$ sequestration traced by sulfur isotopes at Hellisheiði geothermal system, Iceland. Geothermics 83, 101730.
Gylfadóttir, S.S., Kim, J., Helgason, J.K., Brynjólfsson, S., Höskuldsson, Á., Jóhannesson, T., Harbitz, C.B., Løvholt, F., 2017. The 2014 Lake Askja rockslide-induced tsunami: Optimization of numerical tsunami model using observed data. J. Geophys. Res. Oceans 122 (5), 4110–4122.
Halldórsson, S.A., Bali, E., Hartley, M.E., Neave, D.A., Peate, D.W., Guðfinnsson, G.H., Bindeman, I., Whitehouse, M.J., Riishuus, M.S., Pedersen, G.B.M., Jakobsson, S., Askew, R., Gallagher, C.R., Guðmundsdóttir, E.R., Gudnason, J., Moreland, W.M., Óskarsson, B.V., Nikkola, P., Reynolds, H.I., Schmith, J., Thordarson, T., 2018. Petrology and Geochemistry of the 2014–2015 Holuhraun Eruption, Central Iceland: Compositional and Mineralogical Characterist. Temporal Variability and Magma Storage. Contrib. Mineral. Petrol., 173, pp. 1–25.
Halldórsson, S.A., Marshall, E.W., Caracciolo, A., Matthews, S., Bali, E., Rasmussen, M.B., Ranta, E., Gunnarsson Robin, J., Gudfinnsson, G.H., Sigmarsson, O., Maclennan, J., Jackson, M.G., Whitehouse, M., Jeon, H., van der Meer, Q., Mibei, G.K., Kalliokoski, M., Repczynska, M.M., Rúnarsdóttir, R.H., Sigurðsson, G., Pfeffer, M.A., Scott, S.W., Kjartansdóttir, R., Kleine, B.I., Oppenheimer, C., Aiuppa, A., Ilyinskaya, E., Bitetto, M., Giudice, G., Stefánsson, A., 2022. Rapid shifting of a deep magmatic source at Fagradalsfjall volcano, Iceland. Nature 609.
Harðardóttir, S., Halldórsson, S.A., Hilton, D.R., 2018. Spatial distribution of helium isotopes in Icelandic geothermal fluids and volcanic materials with implications for location, upwelling and evolution of the Icelandic mantle plume. Chem. Geol. 480, 12–27.
Hartley, M.E., Thordarson, T., 2012. Formation of Öskjuvatn caldera at Askja, North Iceland: Mechanism of caldera collapse and implications for the lateral flow hypothesis. J. Volcanol. Geotherm. Res. 227, 85–101.
Hartley, M.E., De Hoog, J.C., Shorttle, O., 2021. Boron isotopic signatures of melt inclusions from North Iceland reveal recycled material in the Icelandic mantle source. Geochim. Cosmochim. Acta 294, 273–294.
Hernández, P.A., Pérez, N.M., Fridriksson, T., Egbert, J., Ilyinskaya, E., Thárhallsson, A., Ívarsson, G., Gíslason, G., Gunnarsson, I., Jónsson, B., Padrón, E., Melián, G., Mori, T., Notsu, K., 2012. Diffuse volcanic degassing and thermal energy release from Hengill volcanic system, Iceland. Bull. Volcanol. 74 (10), 2435–2448.
Hilton, D.R., 1996. The helium and carbon isotope systematics of a continental geothermal system: results from monitoring studies at Long Valley caldera (California, USA). Chem. Geol. 127 (4), 269–295.
Horita, J., Wesolowski, D.J., 1994. Liquid-vapor fractionation of oxygen and hydrogen isotopes of water from the freezing to the critical temperature. Geochim. Cosmochim. Acta 58 (16), 3425–3437.
Iacovino, K., Matthews, S., Wieser, P.E., Moore, G.M., Bégué, F., 2021. VESIcal Part I: an open-source thermodynamic model engine for mixed volatile ($H_2O$-$CO_2$) solubility in silicate melts. *Earth and Space*. Science 8 (11) e2020EA001584.
Ilyinskaya, E., Aiuppa, A., Bergsson, B., Di Napoli, R., Fridriksson, T., Óladottir, A.A., Óskarsson, F., Grassa, F., Pfeffer, M., Lechner, K., Yeo, R., Giudice, G., 2015. Degassing regime of Hekla volcano 2012–2013. Geochim. Cosmochim. Acta 159, 80–99.
Ilyinskaya, E., Mobbs, S., Burton, R., Burton, M., Pardini, F., Pfeffer, M.A., Purvis, R., Lee, J., Bauguitte, S., Brooks, B., Colfescu, I., Petersen, G.N., Wellpott, A., Bergsson, B., 2018. Globally significant $CO_2$ emissions from Katla, a subglacial volcano in Iceland. Geophys. Res. Lett. 45 (19), 10–332.
Javoy, M., Pineau, F., Iiyama, I., 1978. Experimental determination of the isotopic fractionation between gaseous CO2 and carbon dissolved in tholeiitic magma. Contrib. Mineral. Petrol. 67 (1), 35–39.
Jenkins, J., Maclennan, J., Green, R.G., Cottaar, S., Deuss, A.F., White, R.S., 2018. Crustal formation on a spreading ridge above a mantle plume: receiver function imaging of the Icelandic crust. J. Geophys. Res. Solid Earth 123 (6), 5190–5208.
Jóhannesson, T., Pálmason, B., Hjartarson, Á., Jarosch, A.H., Magnússon, E., Belart, J.M., Gudmundsson, M.T., 2020. Non-surface mass balance of glaciers in Iceland. J. Glaciol. 66 (258), 685–697.
Jónasson, K., Einarsson, S., 2009. Jarðminjar á háhitasvæðum Íslands: jarðfræði, landmótun og yfirborðsummerki jarðhita. Icelandic Institute of Natural History internal report, NÍ-09012, 151 pp (in Icelandic).
Kleine, B.I., Stefansson, A., Halldórsson, S.A., Barnes, J.D., 2020. Impact of fluid-rock interaction on water uptake of the Icelandic crust: Implications for the hydration of the oceanic crust and the subducted water flux. Earth Planet. Sci. Lett. 538, 116210.
Kleine, B.I., Gunnarsson-Robin, J., Kamunya, K.M., Ono, S., Stefánsson, A., 2021. Source controls on sulfur abundance and isotope fractionation in hydrothermal fluids in the Olkaria geothermal field, Kenya. Chem. Geol. 582, 120446.
Kleine, B.I., Stefánsson, A., Zierenberg, R.A., Jeon, H., Whitehouse, M.J., Jónasson, K., Fridleifsson, G.Ó., Weisenberger, T.B., 2022. Sulfate (re-) cycling in the oceanic crust: Effects of seawater-rock interaction, sulfur reduction and temperature on the abundance and isotope composition of anhydrite. Geochim. Cosmochim. Acta 317, 65–90.
Labidi, J., Barry, P.H., Bekaert, D.V., Broadley, M.W., Marty, B., Giunta, T., Warr, O., Sherwood Lollar, B., Fischer, T.P., Avice, G., Caracausi, A., Ballentine, C.J., Halldórsson, S.A., Stefánsson, A., Kurz, M.D., Kohl, I.E., Young, E.D., 2020. Hydrothermal $^{15}N^{15}N$ abundances constrain the origins of mantle nitrogen. Nature 580 (7803), 367–371.
Maclennan, J., 2019. Mafic tiers and transient mushes: evidence from Iceland. Phil. Trans. R. Soc. A 377 (2139), 20180021.
Macpherson, C., Mattey, D., 1994. Carbon isotope variations of $CO_2$ in Central Lau Basin basalts and ferrobasalts. Earth Planet. Sci. Lett. 121 (3–4), 263–276.
Mandeville, C.W., Webster, J.D., Tappen, C., Taylor, B.E., Timbal, A., Sasaki, A., Hauri, E., Bacon, C.R., 2009. Stable isotope and petrologic evidence for open-system degassing during the climactic and pre-climactic eruptions of Mt. Mazama, Crater Lake, Oregon. Geochim. Cosmochim. Acta 73 (10), 2978–3012.
Marini, L., Moretti, R., Accornero, M., 2011. Sulfur isotopes in magmatic-hydrothermal systems, melts, and magmas. Rev. Mineral. Geochem. 73 (1), 423–492.
Marshall, E.W., Ranta, E., Halldórsson, S.A., Caracciolo, A., Bali, E., Jeon, H., Whitehouse, M.J., Barnes, J.D., Stefánsson, A., 2022. Boron isotope evidence for de-volatilized and rehydrated recycled materials in the Icelandic mantle source. Earth Planet. Sci. Lett. 577, 117229.
Marty, B., Giggenbach, W.F., 1990. Major and rare gases at White Island volcano, New Zealand: origin and flux of volatiles. Geophys. Res. Lett. 17 (3), 247–250.
Marty, B., Zimmermann, L., 1999. Volatiles (he, C, N, Ar) in mid-ocean ridge basalts: Assesment of shallow-level fractionation and characterization of source composition. Geochim. Cosmochim. Acta 63 (21), 3619–3633.
Matthews, S., Shorttle, O., Maclennan, J., Rudge, J.F., 2021. The global melt inclusion C/Ba array: Mantle variability, melting process, or degassing? Geochim. Cosmochim. Acta 293, 525–543.
McGee, K.A., Doukas, M.P., Gerlach, T.M., 2001. Quiescent hydrogen sulfide and carbon dioxide degassing from Mount Baker, Washington. Geophys. Res. Lett. 28 (23), 4479–4482.
Mitchell, M.A., White, R.S., Roecker, S., Greenfield, T., 2013. Tomographic image of melt storage beneath Askja Volcano, Iceland using local microseismicity. Geophys. Res. Lett. 40 (19), 5040–5046.
Montanaro, C., Scheu, B., Gudmundsson, M.T., Vogfjörd, K., Reynolds, H.I., Dürig, T., Strehlow, K., Rott, S., Reuschlé, T., Dingwell, D.B., 2016. Multidisciplinary constraints of hydrothermal explosions based on the 2013 Gengissig lake events, Kverkfjöll volcano, Iceland. Earth Planet. Sci. Lett. 434, 308–319.
Mortensen, A.K., Egilson, Þ., Gautason, B., Árnadóttir, S., Guðmundsson, Á., 2014. Stratigraphy, alteration mineralogy, permeability and temperature conditions of well IDDP-1, Krafla, NE, Iceland. Geothermics 49, 31–41.
Neave, D.A., Putirka, K.D., 2017. A new clinopyroxene-liquid barometer, and implications for magma storage pressures under Icelandic rift zones. Am. Mineral. 102 (4), 777–794.
Oddsson, B., 2016. Heat Transfer in Volcanic Settings: Application to Lava-Ice Interaction and Geothermal Areas. PhD dissertation,. Faculty of Earth Science, University of Iceland, 106 pp.
Ohmoto, H., Lasaga, A.C., 1982. Kinetics of reactions between aqueous sulfates and sulfides in hydrothermal systems. Geochim. Cosmochim. Acta 46 (10), 1727–1745.
Óladóttir, B.A., Larsen, G., Sigmarsson, O., 2011. Holocene volcanic activity at Grímsvötn, Bárdarbunga and Kverkfjöll subglacial centres beneath Vatnajökull, Iceland. Bull. Volcanol. 73 (9), 1187–1208.
Ólafsson, J., 1980. Temperature structure and water chemistry of the caldera Lake Öskjuvatn, Iceland. Limnol. Oceanogr. 25 (5), 779–788.
Ólafsson, M., Torfason, H., Grönvold, K., 2000. Surface exploration and monitoring of geothermal activity in the Kverkfjöll geothermal area, Central Iceland. Proceed. Geothermal Congress, Kyushu-Tohohu, Japan 28, 1539–1545.
Ono, S., Shanks III, W.C., Rouxel, O.J., Rumble, D., 2007. S-33 constraints on the seawater sulfate contribution in modern seafloor hydrothermal vent sulfides. Geochim. Cosmochim. Acta 71 (5), 1170–1182.
Ono, S., Keller, N.S., Rouxel, O., Alt, J.C., 2012. Sulfur-33 constraints on the origin of secondary pyrite in altered oceanic basement. Geochim. Cosmochim. Acta 87, 323–340.
Parkhurst, D.L., Appelo, C.A.J., 1999. User's guide to PHREEQC (Version 2): A computer program for speciation, batch-reaction, one-dimensional transport, and inverse geochemical calculations. Water Res. Investigat. Rep. 99 (4259), 312.
Parmigiani, A., Degruyter, W., Leclaire, S., Huber, C., Bachmann, O., 2017. The mechanics of shallow magma reservoir outgassing. Geochem. Geophys. Geosyst. 18 (8), 2887–2905.
Pedersen, G.B.M., Höskuldsson, A., Dürig, T., Thordarson, T., Jonsdottir, I., Riishuus, M. S., Óskarsson, B.H., Dumont, S., Magnusson, E., Gudmundsson, M.T., Sigmundsson, F., Drouin, V.J.P.B., Gallagher, C., Askew, R., Gudnason, J., Moreland, W.M., Nikkola, P., Reynolds, H.I., Schmith, J., the IES eruption team, 2017. Lava field evolution and emplacement dynamics of the 2014–2015 basaltic fissure eruption at Holuhraun, Iceland. J. Volcanol. Geotherm. Res. 340, 155–169.
Pedersen, G.B., Belart, J.M., Óskarsson, B.V., Gudmundsson, M.T., Gies, N., Högnadóttir, T., Hjartardóttir, A.R., Pinel, V., Berthier, E., Dürig, T., Reynolds, H.I., Hamilton, C.W., Valsson, G., Einarsson, P., Ben-Yehoshua, D., Gunnarsson, A., Oddsson, B., 2022. Volume, effusion rate, and lava transport during the 2021 Fagradalsfjall eruption: results from near real-time photogrammetric monitoring. Geophys. Res. Lett. 49 (13) e2021GL097125.
Poreda, R.J., Craig, H., Arnorsson, S., Welhan, J.A., 1992. Helium isotopes in Icelandic geothermal systems: I. 3He, gas chemistry, and 13C relations. Geochim. Cosmochim. Acta 56 (12), 4221–4228.
Ranta, E., 2022. Stable Isotopes of Volatile Elements as a Window into the Crust and Mantle beneath Icelandic Volcanoes. PhD dissertation. University of Iceland, 217 pp.
Ranta, E., Barnes, J.D., Halldórsson, S.A., Jónasson, K., Stefánsson, A., 2021. Chlorine isotope ratios record magmatic brine assimilation during rhyolite genesis. Geochem. Perspect. Letters 16, 35–39.
Ranta, E., Gunnarsson-Robin, J., Halldórsson, S.A., Ono, S., Izon, G., Jackson, M.G., Reekie, C.D.J., Jenner, F.E., Guðfinnsson, G.H., Jónsson, O.P., Stefánsson, A., 2022. Ancient and recycled sulfur sampled by the Iceland mantle plume. Earth Planet. Sci. Lett. 584, 117452.
Ricci, A., Kleine, B.I., Fiebig, J., Gunnarsson-Robin, J., Kamunya, K.M., Mountain, B., Stefánsson, A., 2022. Equilibrium and kinetic controls on molecular hydrogen abundance and hydrogen isotope fractionation in hydrothermal fluids. Earth Planet. Sci. Lett. 579, 117338.

Sakai, H., Matsubaya, O., 1977. Stable isotopic studies of Japanese geothermal systems. Geothermics 5 (1–4), 97–124.
Sano, Y., Marty, B., 1995. Origin of carbon in fumarolic gas from island arcs. Chem. Geol. 119 (1–4), 265–274.
Seward, T.M., Kerrick, D.M., 1996. Hydrothermal $CO_2$ emission from the Taupo volcanic zone, New Zealand. Earth Planet. Sci. Lett. 139 (1–2), 105–113.
Shinohara, H., 2013. Volatile flux from subduction zone volcanoes: Insights from a detailed evaluation of the fluxes from volcanoes in Japan. J. Volcanol. Geotherm. Res. 268, 46–63.
Sigurgeirsson, M.A., Hjartarson, Á., Kaldal, I., Sæmundsson, K., Kristinsson, S.G., Víkingsson, S., 2015. Geological Map of the Northern Volcanic Zone, Iceland. Southern Part. 1:100 000. Iceland GeoSurvey, Reykjavík.
Sparks, R.S.J., Wilson, L., Sigurdsson, H., 1981. The pyroclastic deposits of the 1875 eruption of Askja, Iceland. Philos. Transact. Royal Soc. London. Series A, Math. Phys. Sci. 299 (1447), 241–273.
Stefánsson, A., 2017. Gas chemistry of Icelandic thermal fluids. J. Volcanol. Geotherm. Res. 346, 81–94.
Stefánsson, A., Arnórsson, S., 2000. Feldspar saturation state in natural waters. Geochim. Cosmochim. Acta 64 (15), 2567–2584.
Stefánsson, A., Arnórsson, S., 2002. Gas pressures and redox reactions in geothermal fluids in Iceland. Chem. Geol. 190 (1–4), 251–271.
Stefánsson, A., Barnes, J.D., 2016. Chlorine isotope geochemistry of Icelandic thermal fluids: Implications for geothermal system behavior at divergent plate boundaries. Earth Planet. Sci. Lett. 449, 69–78.
Stefansson, A., Gunnarsson, I., Giroud, N., 2007. New methods for the direct determination of dissolved inorganic, organic and total carbon in natural waters by Reagent-FreeTM Ion Chromatography and inductively coupled plasma atomic emission spectrometry. Anal. Chim. Acta 582 (1), 69–74.
Stefánsson, A., Arnórsson, S., Gunnarsson, I., Kaasalainen, H., Gunnlaugsson, E., 2011. The geochemistry and sequestration of $H_2S$ into the geothermal system at Hellisheidi, Iceland. J. Volcanol. Geotherm. Res. 202 (3–4), 179–188.
Stefánsson, A., Keller, N.S., Robin, J.G., Ono, S., 2015. Multiple sulfur isotope systematics of Icelandic geothermal fluids and the source and reactions of sulfur in volcanic geothermal systems at divergent plate boundaries. Geochim. Cosmochim. Acta 165, 307–323.
Stefánsson, A., Keller, N.S., Robin, J.G., Kaasalainen, H., Björnsdóttir, S., Pétursdóttir, S., Jóhannesson, H., Hreggvidsson, G.Ó., 2016a. Quantifying mixing, boiling, degassing, oxidation and reactivity of thermal waters at Vonarskard, Iceland. J. Volcanol. Geotherm. Res. 309, 53–62.
Stefánsson, A., Sveinbjörnsdóttir, Á.E., Heinemeier, J., Arnórsson, S., Kjartansdóttir, R., Kristmannsdóttir, H., 2016b. Mantle $CO_2$ degassing through the Icelandic crust: evidence from carbon isotopes in groundwater. Geochim. Cosmochim. Acta 191, 300–319.
Stefánsson, A., Hilton, D.R., Sveinbjörnsdóttir, Á.E., Torssander, P., Heinemeier, J., Barnes, J.D., Ono, S., Halldórsson, S.A., Fiebig, J., Arnórsson, S., 2017. Isotope systematics of Icelandic thermal fluids. J. Volcanol. Geotherm. Res. 337, 146–164.
Taran, Y.A., 2009. Geochemistry of volcanic and hydrothermal fluids and volatile budget of the Kamchatka–Kuril subduction zone. Geochim. Cosmochim. Acta 73 (4), 1067–1094.
Taran, Y., Kalacheva, E., 2019. Role of hydrothermal flux in the volatile budget of a subduction zone: Kuril arc, Northwest Pacific. Geology 47 (1), 87–90.
Taran, Y., Zelenski, M., Chaplygin, I., Malik, N., Campion, R., Inguaggiato, S., Pokrovsky, B., Kalacheva, E., Melnikov, D., Kazahaya, R., Fischer, T., 2018. Gas emissions from volcanoes of the Kuril Island arc (NW Pacific): geochemistry and fluxes. Geochem. Geophys. Geosyst. 19 (6), 1859–1880.
Thode, H.G., Monster, J., Dunford, H.B., 1961. Sulphur isotope geochemistry. Geochim. Cosmochim. Acta 25 (3), 159–174.
Thórarinsson, S., 1953. The Grímsvötn Expedition June-July 1953. Jökull 3, 6–22.
Thórarinsson, S., Sigvaldason, G.E., 1962. The eruption in Askja, 1961; a preliminary report. Am. J. Sci. 260 (9), 641–651.
Thordarson, T., Höskuldsson, Á., 2008. Postglacial volcanism in Iceland. Jökull 58 (198), e228.
Thordarson, T., Larsen, G., 2007. Volcanism in Iceland in historical time: Volcano types, eruption styles and eruptive history. J. Geodyn. 43 (1), 118–152.
Torssander, P., 1989. Sulfur isotope ratios of Icelandic rocks. Contrib. Mineral. Petrol. 102 (1), 18–23.
Truesdell, A.H., Fournier, R.O., 1977. Procedure for estimating the temperature of a hot-water component in a mixed water by using a plot of dissolved silica versus enthalpy. USGS J. Res. 5, 49–52.
Webster, J.D., 2004. The exsolution of magmatic hydrosaline chloride liquids. Chem. Geol. 210 (1–4), 33–48.
Webster, J.D., Vetere, F., Botcharnikov, R.E., Goldoff, B., McBirney, A., Doherty, A.L., 2015. Experimental and modeled chlorine solubilities in aluminosilicate melts at 1 to 7000 bars and 700 to 1250 C: applications to magmas of Augustine Volcano, Alaska. Am. Mineral. 100 (2–3), 522–535.
White, S.M., Crisp, J.A., Spera, F.J., 2006. Long-term volumetric eruption rates and magma budgets. Geochem. Geophys. Geosyst. 7 (3).
White, R.S., Edmonds, M., Maclennan, J., Greenfield, T., Agustsdottir, T., 2019. Melt movement through the Icelandic crust. Phil. Trans. R. Soc. A 377 (2139), 20180010.
Witham, F., Blundy, J., Kohn, S.C., Lesne, P., Dixon, J., Churakov, S.V., Botcharnikov, R., 2012. SolEx: A model for mixed COHSCl-volatile solubilities and exsolved gas compositions in basalt. Comput. Geosci. 45, 87–97.